Experimental investigation of the effect of nitrogen on the phase equilibrium behavior of the CH4–CO2 mixture at low temperature for natural and biogas purification

Marco Campestrini, Francesca Rabino, David Marques, Dyhia Atig, Paolo Stringari, Guido Franzoni, Barbara Picutti

Experimental investigation of the effect of nitrogen on the phase equilibrium behavior of the CH_4-CO_2 mixture at low temperature for natural and biogas purification

Marco Campestrini[a]*, *Francesca Rabino*[b], *David Marques*[a], *Dyhia Atig*[a], *Paolo Stringari*[a], *Guido Franzoni*[b], *Barbara Picutti*[b]

AUTHOR ADDRESS

a – MINES ParisTech, PSL University, CTP – Centre of Thermodynamics of Processes, 35 rue St Honoré 77300 Fontainebleau, France

b – Tecnimont S.p.A., via Gaetano De Castillia 6/A, 20124 Milan, Italy

*Corresponding Author: marco.campestrini@mines-paristech.fr

ABSTRACT

New fluid-fluid and solid-fluid(-fluid) equilibrium measurements at 4 MPa for the N_2 + CH_4 + CO_2 system have been carried out using a static-analytic method in order to investigate the effect of nitrogen on the phase equilibrium behavior of the methane + carbon dioxide mixture at temperatures between 170 K and 210 K. With respect to equilibria involving solid carbon dioxide, the addition of nitrogen to the mixture reduces the solubility of carbon dioxide in the fluid phase, widens the temperature region of existence of the solid-vapor equilibrium, and spreads the temperature range of existence of the solid-liquid-vapor equilibrium. The comparison between measured values and values calculated by means of the Peng-Robinson Equation of State as implemented in Aspen HYSYS® shows that tabulated binary interaction parameters (regressed with respect to fluid-fluid equilibria) are not always suitable when applied to the calculation of low temperature equilibria.

Keywords: Natural gas, biogas, nitrogen, low temperature, phase equilibrium

1. Introduction

Natural gas is expected to play an important two-fold role in the energy transition: supporting coal-switching in fast developing countries and providing a source of low-carbon power when combined with CCUS, either as a direct energy source for power and industrial sectors or to produce blue hydrogen [1]. In addition, biogas and biomethane are going to largely contribute to the low-carbon economy, arriving at covering 20% of current worldwide gas demand at full utilization of the sustainable potential [2].

Natural gas is a mixture of hydrocarbons and non-hydrocarbon species, including acid gases (such as CO_2 and H_2S), water and inert gases (e.g., nitrogen), whose contents vary depending on the characteristics of gas fields [3]. CO_2, N_2 and water are also the main contaminants of raw biogas [4], which is basically composed of methane (55-70%), CO_2 (30-45%), and nitrogen (up to 15%), with small amounts of oxygen, ammonia, and hydrogen sulfide [5].

In both natural gas and biogas, contaminants must be removed before any eventual use. Among the existing purification technologies, cryogenic processes have drawn attention for gas treatment and biogas upgrading applications, especially if coupled with the production of LNG or LBM (liquid biomethane) and with other cryogenic processes (such as Nitrogen Rejection), thanks to the possibility of minimizing energy consumption through the integration of cryogenic purification and gas liquefaction [6,7].

At the low operative temperatures of cryogenic purification processes, CO_2 solidification can occur, leading to plugging, equipment blockage, ruptures and failures, turning into higher safety risks and plant reduced availability. Accurate and reliable predictions of the thermodynamic behavior of gas mixtures are essential to allow effective and safe design of cryogenic systems in

which CO_2 freezing conditions are to be avoided. Despite this strong constraint, only few commercial process simulators, widely used for cryogenic units' process design, are able to make solid-fluid equilibria calculations. To overcome this limitation, some simulators include built-in packages which, however, are reported to inaccurately predict solid CO_2 formation [8,9]. Moreover, given binary interaction parameters (k_{ij}) may not be adequate to describe the phase equilibria existing in the pressure-temperature range to be simulated [10].

Consequently, the accuracy of thermodynamic models commonly embedded in process simulators in properly representing the thermodynamic behavior of gaseous mixtures containing N_2, CH_4 and CO_2 at the desired conditions, needs to be improved.

In this work, original Vapor-Liquid Equilibrium (VLE), Solid-Liquid Equilibrium (SLE), Solid-Vapor Equilibrium (SVE), and Solid-Liquid-Vapor Equilibrium (SLVE) conditions have been measured for the CH_4 + CO_2 mixture and two N_2 + CH_4 + CO_2 mixtures. Measurements focused on the description of the phase equilibrium behavior of these mixtures in the low temperature (between 170 K and 210 K) – high pressure (close to the critical-point pressure of methane) region of interest for cryogenic processes. Original measurements have then been compared with modeling results obtained by means of a thermodynamic package given by the Peng-Robinson Equation of State [11] (PR EoS), as implemented in Aspen HYSYS® [12], coupled with the classical approach for calculating the fugacity of pure carbon dioxide in the solid state [13].

Modeling results show that, for the natural gas mixtures object of the present investigation, the selected thermodynamic package is inaccurate to predict SLE conditions. The regression of the binary interaction parameters (in particular for the CH_4 + CO_2 system), could lead to the

improvement of the representation of SLE data, keeping at the same time an appropriate representation of the other phase equilibria.

2. Available equilibrium data for the N_2 + CH_4 + CO_2 system

The first experimental works appeared in the open literature dealing with the phase equilibrium behavior of the N_2 + CH_4 + CO_2 system date back to the beginning of the '70s.

VLE data were published by Sarashina et al. [14], Somait and Kidnay [15], Al-Sahhaf et al. [16], Trappehl and Knapp [17], Al-Sahhaf [18], Xu et al. [19], and Xu et al. [20] between 1971 and 1992, and more recently by Ottovy et al. for CO_2 capture and storage applications (VLE of carbon dioxide-rich mixtures) [21].

SVE data were published in 1972 by Haufe et al. (for nitrogen-rich mixtures) [22], in 1974 by Agrawal and Laverman [23], and more recently by Le and Trebble [24], and Xiong et al. [25].

Shen et al. [26] and Gao et al. [27] reported the composition of the liquid phase of the mixture at SLVE conditions in 2012, whereas no information about the vapor composition at the SLVE of the mixture was available before Riva and Stringari published some points between 124 K and 146 K in 2018 [28].

All the experimental pressures and temperatures of the aforementioned VLE, SVE, and SLVE data of the ternary system are illustrated in the pressure-temperature diagram shown in Fig. 1; some additional details (like form of the dataset, pressure and temperature ranges, and number of experimental points for each literature work) are gathered in Table 1.

In Fig. 1, symbols represent the literature values: filled circles are related to all the available VLE data [14-21], empty squares are related to all the available SVE data [22-25], whereas filled triangles are related to all the available SLVE data [26-28].

Furthermore, the saturation line of nitrogen (dotted line), the saturation and melting lines of methane (bold lines), and the sublimation, melting, and saturation lines of carbon dioxide (dashed lines) calculated from [29] have been drawn in Fig. 1 for the reader convenience.

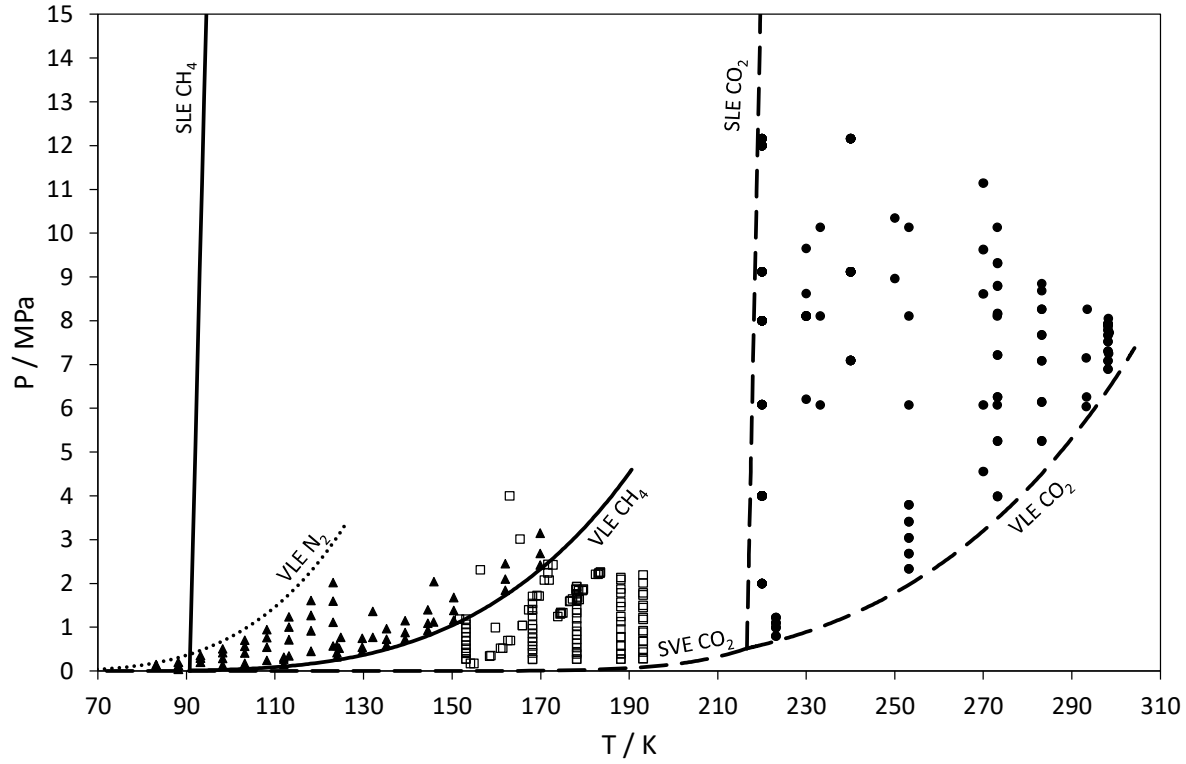

Fig. 1. Pressure-temperature conditions of the phase equilibrium values available in the literature for the $N_2 + CH_4 + CO_2$ system.
● : VLE data; □ : SVE data; ▲ : SLVE data. ••• : VLE line of N_2 [29]; — : SLE and VLE lines of CH_4 [29]; – – : SVE, SLE, and VLE lines of CO_2 [29].

According to the reciprocal position of the available literature data and the boundary equilibrium conditions (saturation, melting, and sublimation) of the three pure components, it is possible to state that (i) VLE data have been measured only at temperatures higher than the triple-point temperature of carbon dioxide, (ii) almost all the SVE data are delimited by the saturation line of methane (VLE CH_4) and the melting (SLE CO_2) and sublimation (SVE CO_2) lines of carbon

dioxide, and (iii) the SLVE data have been measured only between the saturation line of nitrogen (VLE N_2) and that of methane (VLE CH_4).

In addition to that, the majority of the data involving solid carbon dioxide (SVE and SLVE data) have been measured at pressure lower than 2 MPa. As a consequence, in this work authors have focused on the phase equilibrium behavior of the ternary system at a nominal pressure of 4 MPa between 170 K and 210 K.

Table 1. Literature phase equilibrium values for the (1)N_2 + (2)CH_4 +(3)CO_2.

Reference	Year	Kind of data	Form	N° data	T range / K	P range / MPa
14	1971	VLE	PTxy	48	233 – 273	6.1 – 10.1
15	1978	VLE	PTxy	56	270	4.6 – 11.2
16	1983	VLE	PTxy	37	220 – 240	6.0 – 12.2
17	1989	VLE	PTxy	56	220	2.0 – 12.0
18	1990	VLE	PTxy	26	230 – 250	6.2 – 10.3
19	1992	VLE	PTxy	55	293	6.0 – 8.3
20	1992	VLE	PTxy	30	298	7.2 – 8.0
21	2020	VLE	PTx, PTy	62	223 – 298	0.8 – 9.3
22	1972	SVE	PTy	5	152 – 165	1.0 – 4.0
23	1974	SVE	PTy	19	154 – 173	0.2 – 2.4
24	2007	SVE	PTy	24	174 – 183	1.2 – 2.3
25	2015	SVE	PTy	77	153 – 193	0.2 – 2.0
26	2012	SLVE	PTx	27	112 – 170	0.2 – 3.1
27	2012	SLVE	PTx	31	83 – 123	0.1 – 2.0
28	2018	SLVE	PTxy	3	124 – 146	0.5 – 2.0

Contrarily to the ternary system, the abundance of literature data allows the evaluation of the phase equilibrium behaviors of the corresponding binary mixtures in the same temperature range (170 K < T < 210 K): the N_2 + CH_4 system is characterized only by VLE and only the SVE exists for the N_2 + CO_2 system, whereas the CH_4 + CO_2 system behaves at VLE, SVE, SLE, or SLVE according to system pressure, temperature, and global composition [30].

3. Materials, apparatus, and protocol

This work dealt with the experimental investigation of the fluid-fluid and solid-fluid equilibrium behavior of the nitrogen + methane + carbon dioxide system between 170 K and 210 K. The solubility of carbon dioxide in the fluid phases at VLE, SVE, and SLE has been measured in three different nitrogen + methane mixtures (hereafter called solvents). The nominal molar compositions of nitrogen and methane in these 3 solvents are gathered in Table 2. The last two columns of Table 2 give the compositions of nitrogen and methane in the gas cylinders (supplied by MESSER) that have been used in the experimental campaigns.

Table 2. Molar fraction of nitrogen and methane in the solvents used in this work.

Solvents	**Nominal composition**		**Cylinders' composition**	
	xN_2 [%]	**xCH_4 [%]**	**xN_2 [%]**	**xCH_4 [%]**
Solvent **A**	0	100	0	99.995
Solvent **B**	5	95	5.009	94.991
Solvent **C**	10	90	10.2	89.8

Solvent A (pure methane) has been chosen for the validation of the experimental protocol and the calibration of the experimental devices (temperature probes, pressure transducers, and detector of the gas-chromatograph), by comparing the VLE, SLE, and SVE values obtained in this work for the CH_4 + CO_2 system with literature data in the same temperature and pressure ranges.

Solvents B and C have been then chosen for evaluating the effect of nitrogen on the phase equilibrium behavior with particular attention to the solubility limits of carbon dioxide in the liquid and vapor phases.

The details concerning the pure chemicals (suppliers, CAS numbers and stated purities) are gathered in Table 3.

Table 3. Purities and suppliers of the pure chemicals used in this work.

Chemical Name	CAS number	Purity [mol/mol %]	Source
Nitrogen	7727-37-9	99.999	MESSER
Methane	74-82-8	99.995	MESSER
Carbon dioxide	124-38-9	99.998	MESSER

The equipment used for the evaluation of the phase equilibrium behavior is based on a ″static-analytic″ method with liquid and vapor phase samplings. The equipment is similar to that presented by Campestrini et al. [31] and its flow diagram is presented in Fig. 2.

The sapphire equilibrium cell is totally immersed into an ethanol bath whose temperature is regulated at a certain value by means of a temperature regulator. Two platinum resistance thermometer Pt-100 probes and two pressure transducers (DRUCK type PTX611, range: 0-5 MPa, type PTX611, range: 0-20 MPa) allow temperature and pressure readings via a data acquisition unit (HP34970A). Temperature probes have been calibrated against a 25Ω reference platinum thermometer (Pt25, Hart Scientific), previously calibrated by the Trescal Laboratory following the ITS90 (1990 International Temperature Scale) protocol. Pressure transducers are maintained at constant temperature by means of a heating cartridge and have been calibrated against a Dead Weight Balance (Desgranges & Huot).

Samples of the equilibrium phases within the cell are withdrawn thanks to two electromagnetic ROLSI® samplers, vaporized in the heated chamber of the ROLSI® samplers where they are mixed with the carrier gas (helium) into the transfer line. The samples are thus directly injected into the analytical circuit toward the head of the column (Porapak Q, 80/100 mesh; 1/8" Silcosteel tube, 2m length, 2mm internal diameter, Restek) located in the oven of the gas chromatograph (Perichrom Model PR2100), and finally analyzed by a Thermal Conductivity Detector (TCD) connected to an acquisition system (WINILAB III).

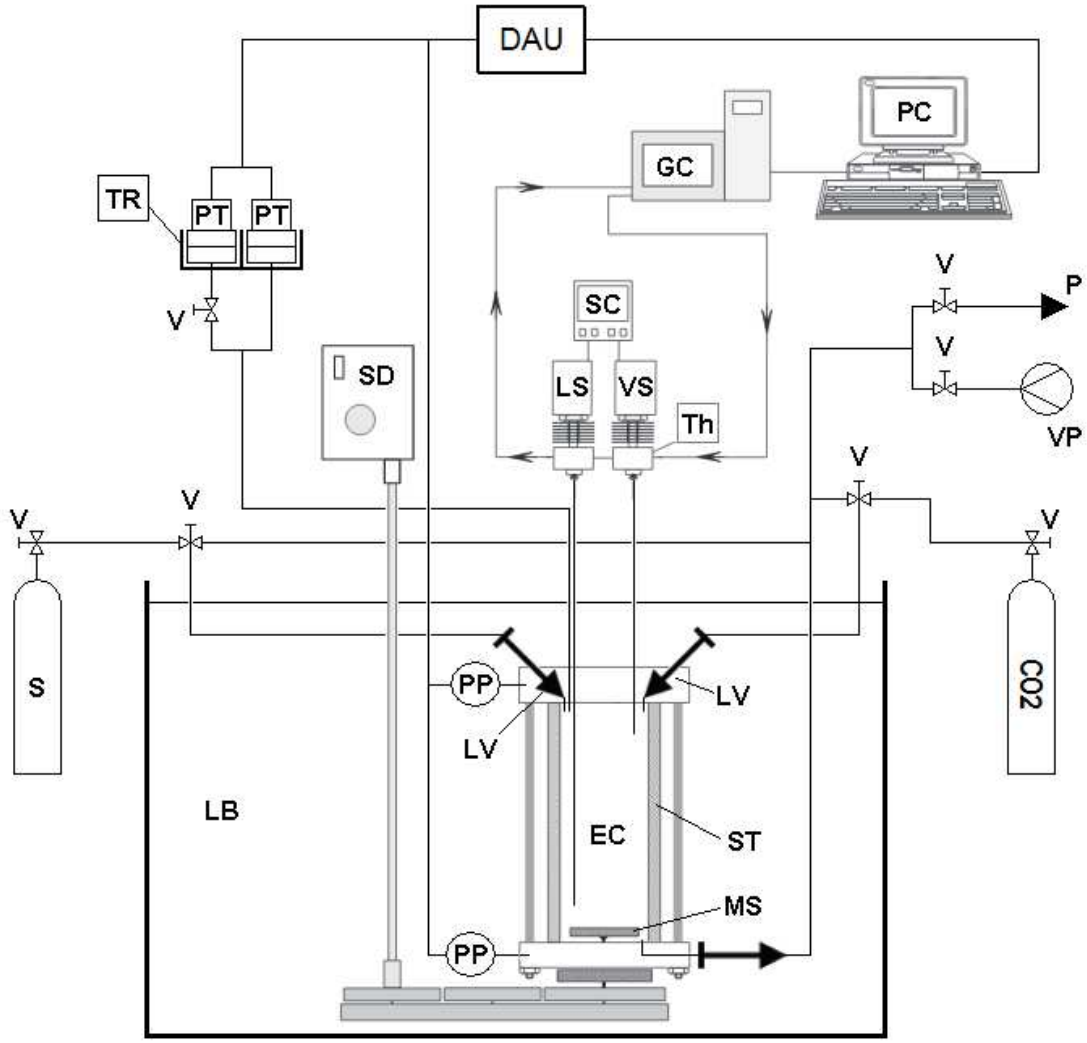

Fig. 2. Flow diagram of the static-analytic apparatus used in this work.
CO2 : carbon dioxide cylinder; DAU : data acquisition unit; EC : equilibrium cell; GC : gas chromatograph; LB : liquid bath (ethanol); LS : liquid ROLSI® sampler; LV: loading valve; MS : magnetic stirrer; P : Purge; PC : personal computer; PP : platinum resistance thermometer probe; PT : pressure transducer; S : gaseous solvent cylinder; SC : sample controller; SD : stirring device; ST : sapphire tube; TR : temperature regulator; Th : thermocouple; V : valve; VP : vacuum pump; VS : vapor ROLSI® sampler.

The equilibrium cell and its loading lines are first evacuated at ambient temperature. The cell is then immersed into the thermo-regulated bath. The temperature of the cell is set to a target value (typically 18°C) by means of the temperature regulator, and adequate stirring is maintained throughout the cell.

A certain pressure of carbon dioxide is then loaded in the cell by opening all the valves between the CO_2 cylinder (CO2 in Fig. 2) and the equilibrium cell. Some solvent is then introduced step-by-step into the cell from the corresponding cylinder, S in Fig. 2, during cooling of the cell until reaching the desired pressure (about 4 MPa) at the first target temperature.

At each target temperature, phase equilibrium is assumed to be achieved when the readings of pressure transducers and temperature probes have stabilized to within their instrument uncertainty for at least 10 minutes.

Once equilibrium is reached, sampling of the equilibrium phases starts while temperature and pressure readings are recorded. The liquid and vapor ROLSI® samplers are used for sampling (i) the liquid phase and vapor phase, respectively, at VLE or SLVE, (ii) the vapor phase at SVE, (iii) the liquid phase at SLE. The samples are then transferred to the GC and analyzed.

The phase equilibrium is considered properly defined once at least six repeatable molar compositions are obtained for both the liquid and the vapor phases.

The temperature of the cell is then successively decreased and further solvent is loaded in the equilibrium cell for increasing the pressure up to the target value. The procedure is then repeated until the target phase equilibrium behavior has been satisfactorily determined or until the lowest experimental temperature has been reached (about 170 K).

4. Results and discussion

In this section, tables gather the experimental values measured in this work according to the system and phase equilibrium. In the tables, temperature is given in K, pressure is given in MPa, compositions of the equilibrium phases are expressed in molar fractions (x is used for the liquid phase, y is used for the vapor phase), expanded and combined standard uncertainties (U) are given for molar fractions, and the experimental points are numbered consecutively. Expanded uncertainty on temperature and pressure is estimated to be 0.004 K and 0.002 MPa, respectively.

The approach adopted for estimating the experimental uncertainties is based on the NIST documentation by Taylor and Kuyatt [32]. Readers can refer to the Supporting Material for details related to the calculation of the uncertainties affecting the experimental results presented in this work.

In this section, figures illustrate the evolution of the carbon dioxide composition in the vapor and liquid phases with temperature at the measured VLE, SVE, and SLE conditions. For graphical purposes, qualitative trend lines have been added in all the figures.

For the solvent A (methane) + carbon dioxide system:

- the measured SVE are gathered in Table 4 and compared to some of the literature SVE values measured by Pikaar [33] in Fig. 3;

- the measured VLE are gathered in Table 5 and compared to some of the literature VLE values measured by Neumann and Walch [34] in Figs. 4 and 5;

- the measured SLE are gathered in Table 6 and compared to the literature SLE and SLVE data [35-46] in Fig. 6.

For the methane + carbon dioxide system, a good qualitative agreement is encountered between all the measured VLE, SVE, and SLE data and the selected literature data.

In the low temperature region (188 K < T < 193 K), the measured solubility of solid CO_2 in vapor methane is slightly lower than the selected values of Pikaar [33] (see Fig. 3).

Table 4. SVE data measured for the solvent A [(1) methane] + (2) carbon dioxide system.

Point	T [K]	P [MPa]	y_1	$U(y_1)$	y_2	$U(y_2)$
1	205.423	4.010	0.8944	0.0039	0.1056	0.0039
2	202.433	4.010	0.9128	0.0033	0.0872	0.0033
3	199.445	4.152	0.9273	0.0028	0.0727	0.0028
4	196.461	4.009	0.9403	0.0023	0.0597	0.0023
5	194.458	4.008	0.9474	0.0022	0.0526	0.0022
6	193.497	4.004	0.9504	0.0021	0.0496	0.0021
7	193.268	4.019	0.9514	0.0020	0.0486	0.0020
8	191.532	4.005	0.9559	0.0018	0.0441	0.0018
9	190.823	3.982	0.9581	0.0019	0.0419	0.0019
10	190.555	4.011	0.9583	0.0015	0.0417	0.0015
11	190.543	4.015	0.9581	0.0018	0.0419	0.0018
12	190.406	4.007	0.9586	0.0015	0.0414	0.0015

U(T) = 0.004 K; U(P) = 0.002 MPa

This deviation could be explained by the slight difference between the experimental pressures (the average SVE pressure of the selected values measured by Pikaar [33] is 3.970 MPa, whereas the average of the pressure given in Table 4 is 4.019 MPa), but this is in contrast with the fact that the solubility is usually expected to increase with increasing pressures.

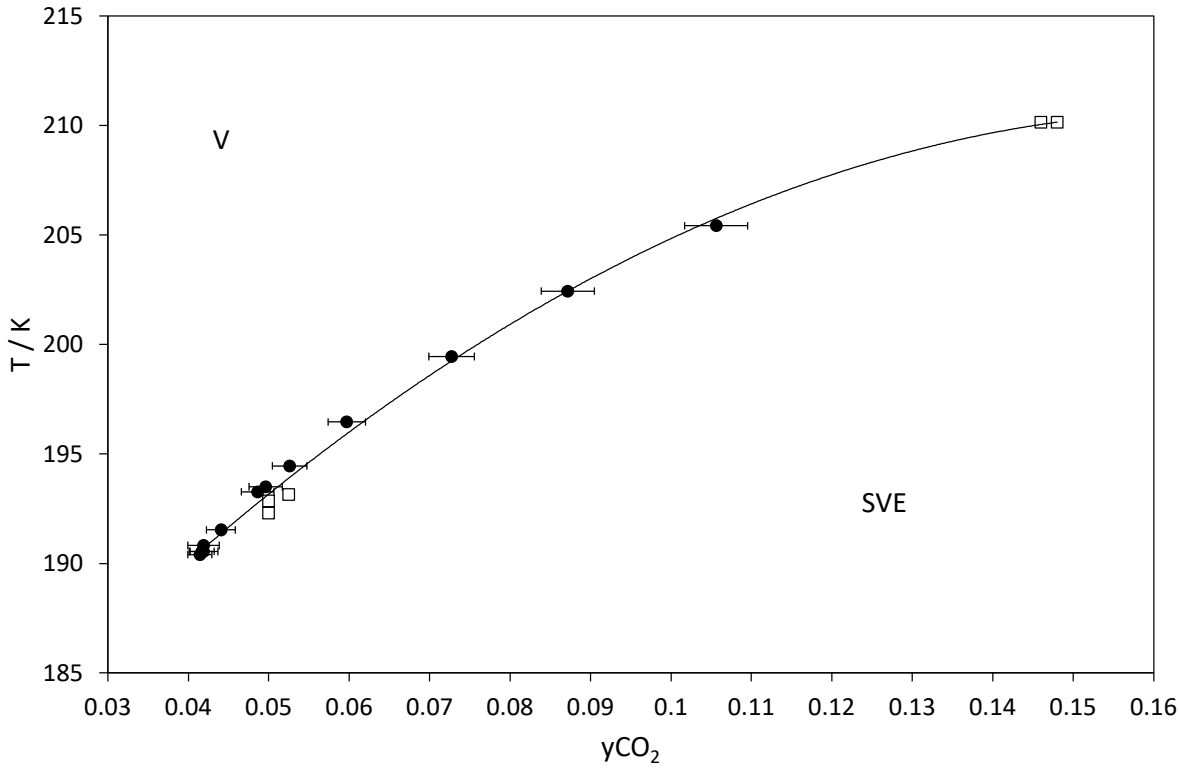

Fig. 3. Experimental solubilities of solid CO_2 in the vapor phase at SVE at 4.019 MPa (average value of points n°1-12) and selected literature data at 3.970 MPa (average value) for the solvent A + CO_2 system.
● : this work; □ : Pikaar [33]; – : trend line.

In Fig. 4, measured VLE compositions of points n°15, n°22, n°23, and n°25 (4.000 MPa average pressure) are compared to a literature value at 4.001 MPa [34]. It should be noticed that the filled triangle in Fig. 4 is at the saturation temperature of methane at (4.008 MPa ± 0.004 MPa) measured in this work (186.121 K ± 0.009 K). Similarly in Fig. 5, measured VLE compositions of points n°16, n°21, and n°24 (3.978 MPa average pressure) are compared to a literature value at 3.982 MPa [34]. According to these comparisons, it is possible to state that part of the measured VLE data given in Table 5 are in a rather good agreement with the data of Neumann and Walch [34].

Table 5. VLE data measured for the solvent A [(1) methane] + (2) carbon dioxide system.

Point	T [K]	P [MPa]	x_1	$U(x_1)$	x_2	$U(x_2)$	y_1	$U(y_1)$	y_2	$U(y_2)$
13	190.293	3.994	0.9045	0.0033	0.0955	0.0033	0.9592	0.0014	0.0408	0.0014
14	190.248	4.015	0.9092	0.0039	0.0908	0.0039	0.9605	0.0016	0.0395	0.0016
15	189.758	4.004	0.9179	0.0026	0.0821	0.0026	0.9638	0.0012	0.0362	0.0012
16	189.742	3.969	0.9106	0.0028	0.0894	0.0028	0.9618	0.0013	0.0382	0.0013
17	189.742	4.031	0.9242	0.0024	0.0758	0.0024	0.9655	0.0012	0.0345	0.0012
18	189.254	3.991	0.9274	0.0023	0.0726	0.0023	0.9673	0.0011	0.0327	0.0011
19	188.857	3.992	0.9368	0.0020	0.0632	0.0020	0.9707	0.0010	0.0293	0.0010
20	188.768	3.991	0.9418	0.0021	0.0582	0.0021	0.9725	0.0011	0.0275	0.0011
21	188.355	3.977	0.9458	0.0018	0.0542	0.0018	0.9744	0.0009	0.0256	0.0009
22	188.335	3.996	0.9502	0.0019	0.0498	0.0019	0.9759	0.0015	0.0241	0.0015
23	187.553	4.000	0.9688	0.0012	0.0312	0.0012	0.9841	0.0006	0.0159	0.0006
24	187.428	3.988	0.9691	0.0012	0.0309	0.0012	0.9842	0.0007	0.0158	0.0007
25	186.936	3.999	0.9822	0.0007	0.0178	0.0007	0.9905	0.0004	0.0095	0.0004

U(T) = 0.004 K; U(P) = 0.002 MPa

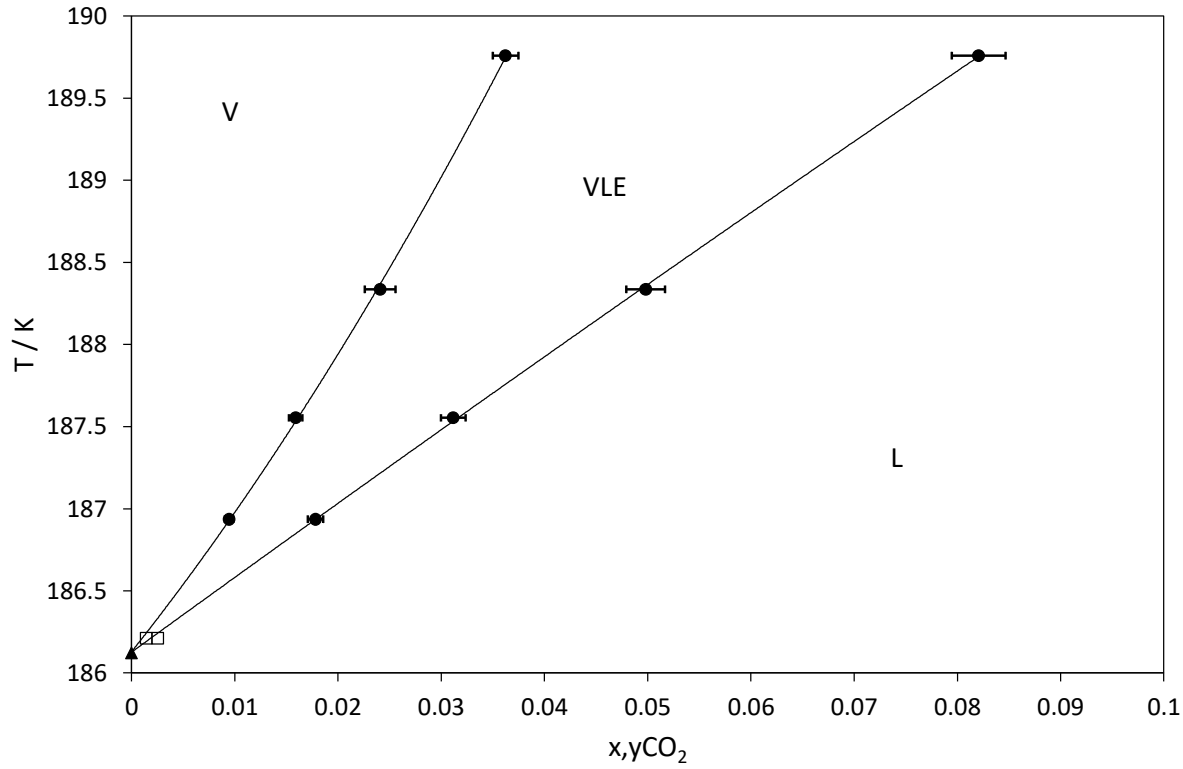

Fig. 4. Experimental compositions of CO_2 in the liquid and vapor phases at VLE at 4.000 MPa (average value of points n°15, n°22, n°23, and n°25) and a selected literature data at 4.001 MPa for the solvent A + CO_2 system.
●,▲ : this work; □ : Neumann and Walch [34]; – : trend lines.

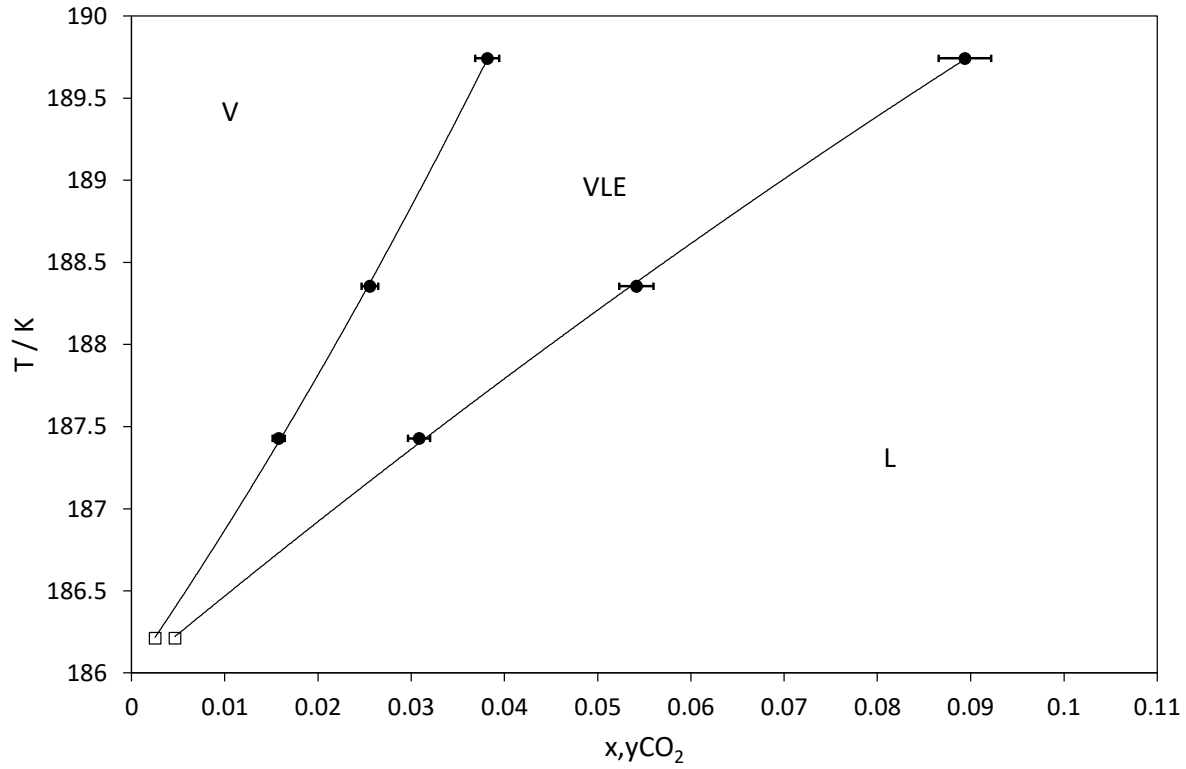

Fig. 5. Experimental compositions of CO_2 in the liquid and vapor phases at VLE at 3.978 MPa (average value of points n°16, n°21, and n°24) and a selected literature data at 3.982 MPa for the solvent A + CO_2 system.
● : this work; □ : Neumann and Walch [34]; – : trend lines.

Measured solubility of carbon dioxide in liquid methane is compared to the solubility of carbon dioxide at SLE and SLVE conditions from the literature [35-46] in the range 170 K < T < 215 K in Fig. 6.

Table 6. SLE data measured for the solvent A [(1) methane] + (2) carbon dioxide system.

Point	T [K]	P [MPa]	x_1	U(x_1)	x_2	U(x_2)
26	189.643	3.969	0.9059	0.0040	0.0941	0.0040
27	188.756	3.996	0.9103	0.0035	0.0897	0.0035
28	185.513	3.984	0.9244	0.0036	0.0756	0.0036
29	182.553	3.993	0.9360	0.0024	0.0640	0.0024
30	179.590	4.006	0.9467	0.0020	0.0533	0.0020
31	176.612	3.931	0.9551	0.0017	0.0449	0.0017

U(T) = 0.004 K; U(P) = 0.002 MPa

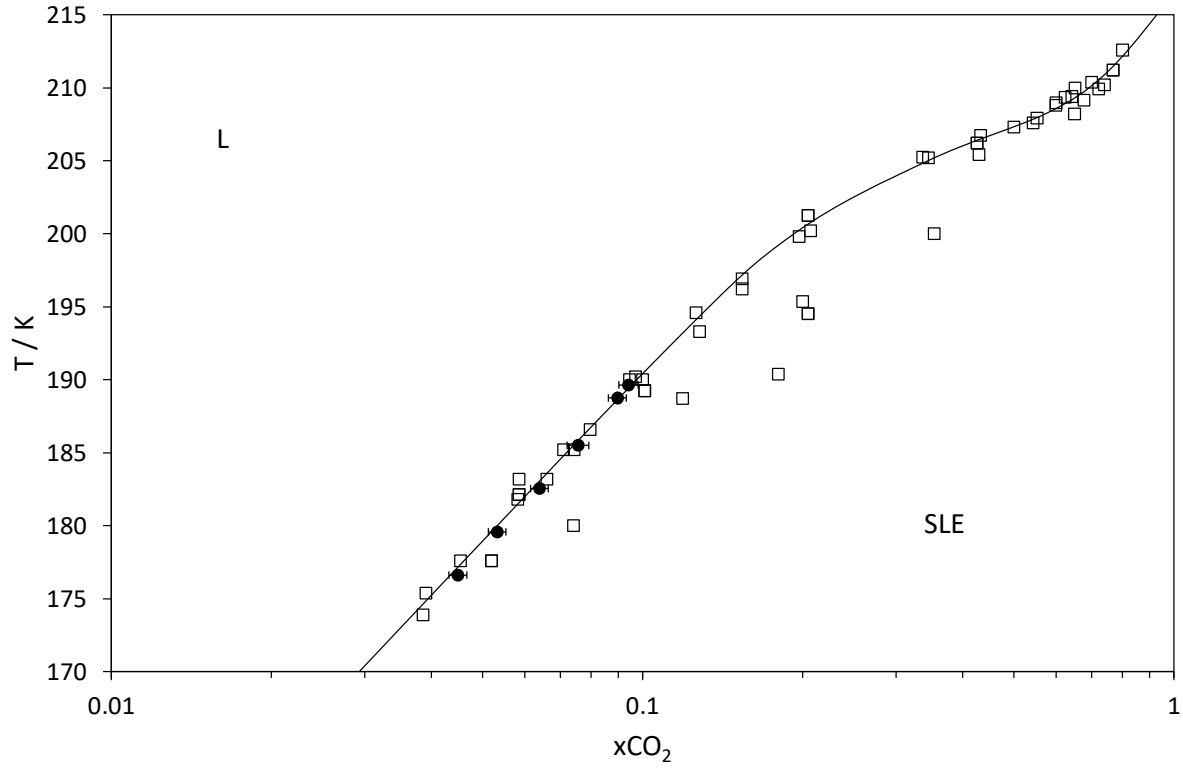

Fig. 6. Experimental solubilities of solid CO_2 in the liquid phase at SLE at 3.980 MPa (average value of points n°26-31) and selected literature SLE and SLVE data in the range 170 K < T < 215 K for the solvent A + CO_2 system.
● : this work; □ : SLE and SLVE data [35-46]; – : trend line.

According to Fig. 6, it is possible to state that measured compositions qualitatively agree with the majority of the literature values as evidenced by the trend line. Unlike the high-temperature region (190 K < T < triple-point temperature of CO_2), regarding all the points shown in Fig. 6 it can be stated that the solubility of solid carbon dioxide in liquid methane almost linearly changes with temperature, from about 4% at 175 K up to about 10% at 190 K.

For the solvent B (5%nitrogen + 95%methane) + carbon dioxide system the measured SVE and SLE are gathered in Table 7 and 8, respectively.

Table 7. SVE data measured for the solvent B [(1) 5%nitrogen + (2) 95%methane] + (3) carbon dioxide system.

Point	T [K]	P [MPa]	y_1	$U(y_1)$	y_2	$U(y_2)$	y_3	$U(y_3)$
32	205.480	3.999	0.0437	0.0020	0.8522	0.0050	0.1041	0.0035
33	202.415	3.995	0.0446	0.0021	0.8698	0.0045	0.0856	0.0029
34	199.406	4.000	0.0452	0.0021	0.8839	0.0041	0.0709	0.0025
35	196.423	3.996	0.0459	0.0021	0.8959	0.0037	0.0582	0.0020
36	193.458	4.006	0.0466	0.0022	0.9052	0.0035	0.0482	0.0017
37	190.462	4.002	0.0469	0.0022	0.9131	0.0033	0.0400	0.0014
38	189.514	3.997	0.0469	0.0022	0.9150	0.0032	0.0381	0.0013
39	188.509	3.999	0.0473	0.0022	0.9165	0.0032	0.0362	0.0013

U(T) = 0.004 K; U(P) = 0.002 MPa

Table 8. SLE data measured for the solvent B [(1) 5%nitrogen + (2) 95%methane] + (3) carbon dioxide system.

Point	T [K]	P [MPa]	x_1	$U(x_1)$	x_2	$U(x_2)$	x_3	$U(x_3)$
40	182.565	4.002	0.0458	0.0022	0.8939	0.0038	0.0603	0.0021
41	181.576	4.002	0.0458	0.0022	0.8969	0.0037	0.0573	0.0020
42	179.551	4.001	0.0462	0.0022	0.9028	0.0035	0.0510	0.0018
43	177.548	3.998	0.0464	0.0022	0.9077	0.0034	0.0459	0.0016
44	176.558	4.001	0.0459	0.0021	0.9109	0.0033	0.0432	0.0015
45	175.767	4.000	0.0460	0.0021	0.9123	0.0033	0.0417	0.0015

U(T) = 0.004 K; U(P) = 0.002 MPa

For the solvent C (10%nitrogen + 90%methane) + carbon dioxide system the measured SVE and SLE are gathered in Table 9 and 10, respectively.

Table 9. SVE data measured for the solvent C [(1) 10%nitrogen + (2) 90%methane] + (3) carbon dioxide system.

Point	T [K]	P [MPa]	y_1	U(y_1)	y_2	U(y_2)	y_3	U(y_3)
46	205.408	3.995	0.0882	0.0037	0.8073	0.0059	0.1045	0.0031
47	202.418	3.993	0.0896	0.0038	0.8248	0.0056	0.0855	0.0026
48	199.413	4.000	0.0911	0.0038	0.8385	0.0052	0.0704	0.0021
49	196.845	3.993	0.0926	0.0039	0.8483	0.0051	0.0591	0.0018
50	196.438	3.997	0.0924	0.0039	0.8499	0.0050	0.0577	0.0018
51	193.467	4.010	0.0935	0.0040	0.8591	0.0049	0.0474	0.0015
52	190.579	3.994	0.0952	0.0045	0.8658	0.0054	0.0390	0.0014
53	190.479	4.004	0.0944	0.0040	0.8670	0.0048	0.0387	0.0012
54	187.496	3.999	0.0956	0.0041	0.8726	0.0047	0.0318	0.0010
55	186.501	4.001	0.0957	0.0041	0.8745	0.0047	0.0298	0.0010
56	185.506	4.001	0.0960	0.0044	0.8758	0.0050	0.0282	0.0010
57	184.521	3.999	0.0968	0.0043	0.8766	0.0048	0.0266	0.0009

U(T) = 0.004 K; U(P) = 0.002 MPa

Table 10. SLE data measured for the solvent C [(1) 10%nitrogen + (2) 90%methane] + (3) carbon dioxide system.

Point	T [K]	P [MPa]	x_1	U(x_1)	x_2	U(x_2)	x_3	U(x_3)
58	178.765	4.003	0.0903	0.0045	0.8625	0.0051	0.0462	0.0016
59	178.496	3.992	0.0906	0.0041	0.8638	0.0051	0.0456	0.0015
60	177.573	4.007	0.0909	0.0039	0.8656	0.0048	0.0435	0.0014
61	176.652	3.995	0.0911	0.0039	0.8673	0.0047	0.0416	0.0013
62	175.721	3.996	0.0920	0.0039	0.8685	0.0047	0.0395	0.0013

U(T) = 0.004 K; U(P) = 0.002 MPa

For the solvents B and C involving nitrogen, all the VLE and SLVE have been grouped together in Table 11 and 12, respectively. In Tables 11 and 12, the molar fraction of nitrogen in the liquid and vapor phase can be calculated as $x_1 = 1 - x_2 - x_3$ and $y_1 = 1 - y_2 - y_3$, respectively.

As shown in Figs. 7 and 8, a first effect of adding nitrogen in the solvent is decreasing the solubility of carbon dioxide in the fluid phase at SVE and SLE. In particular, this effect on the solubility of CO_2 in the vapor phase at SVE appears lower than the one in the liquid at SLE.

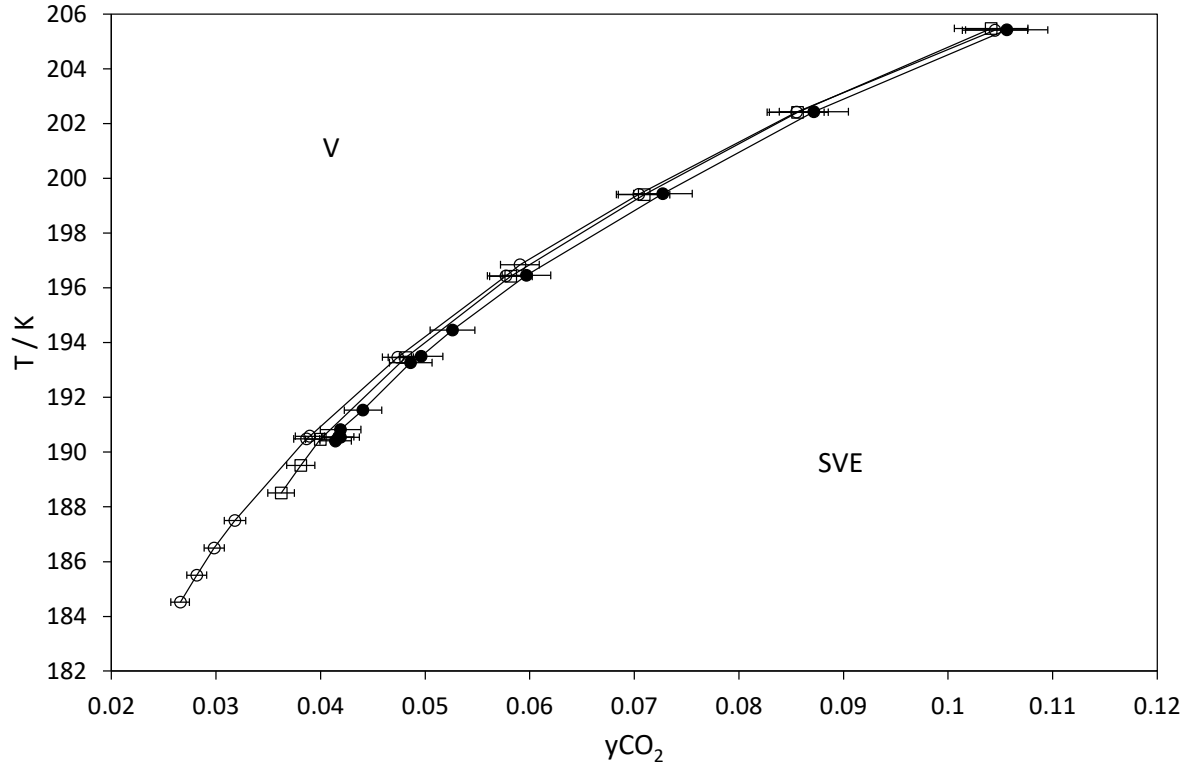

Fig. 7. Effect of nitrogen on the solubility of solid CO_2 in the vapor phase at SVE in the three solvent + CO_2 systems.
● : solvent A; □ : solvent B; ○ : solvent C. Continuous lines are trend lines.

This feature can be explained by taking into account the density of the solvents A, B, and C in the vapor and in the liquid phases and considering that, as a general rule of thumb, the more dense the solvent is, the higher is the solubility.

The densities of solvents A, B, and C as calculated from REFPROP v10 [29] at 4 MPa are shown in Fig. 9 as a function of temperature. It is possible to observe that the densities of solvents B and C in the vapor phase are close to that of solvent A, whereas those in the liquid phase deviate more

from the density of liquid methane. Then the effect of N_2 on the solubility is lower at SVE than at SLE.

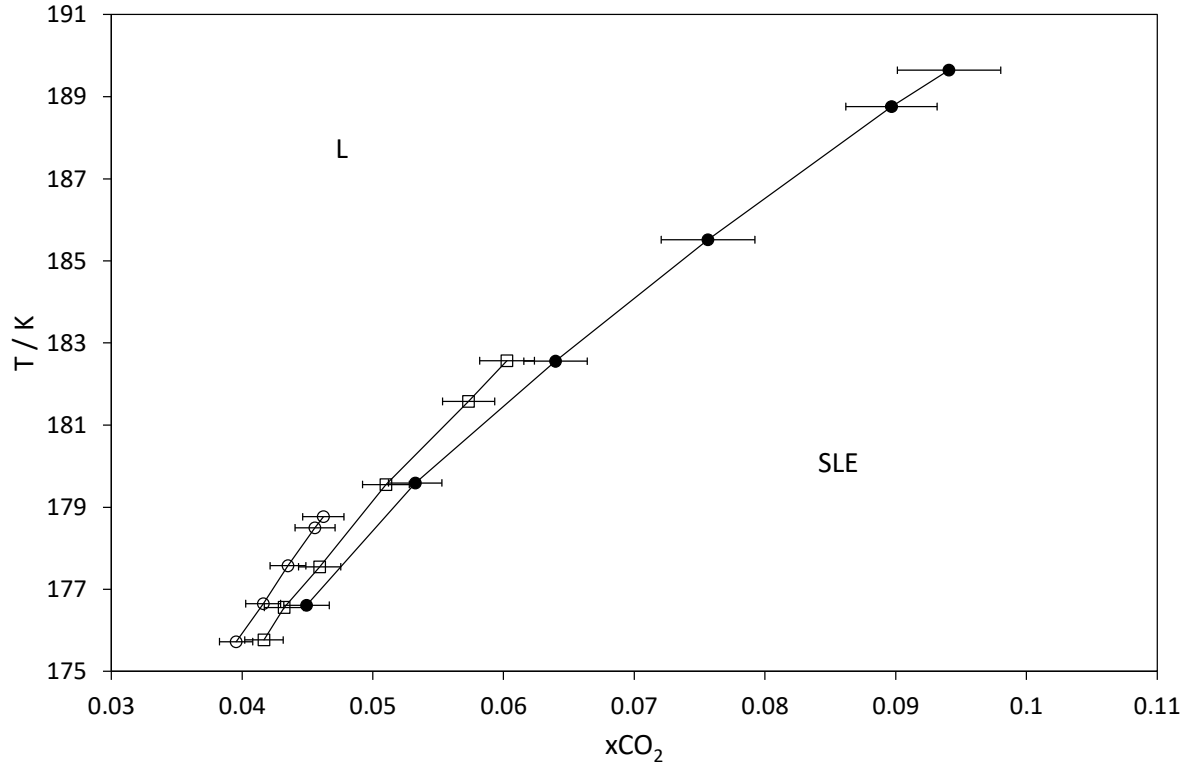

Fig. 8. Effect of nitrogen on the solubility of solid CO_2 in the liquid phase at SLE in the three solvent + CO_2 systems.
● : solvent A; □ : solvent B; ○ : solvent C. Continuous lines are trend lines.

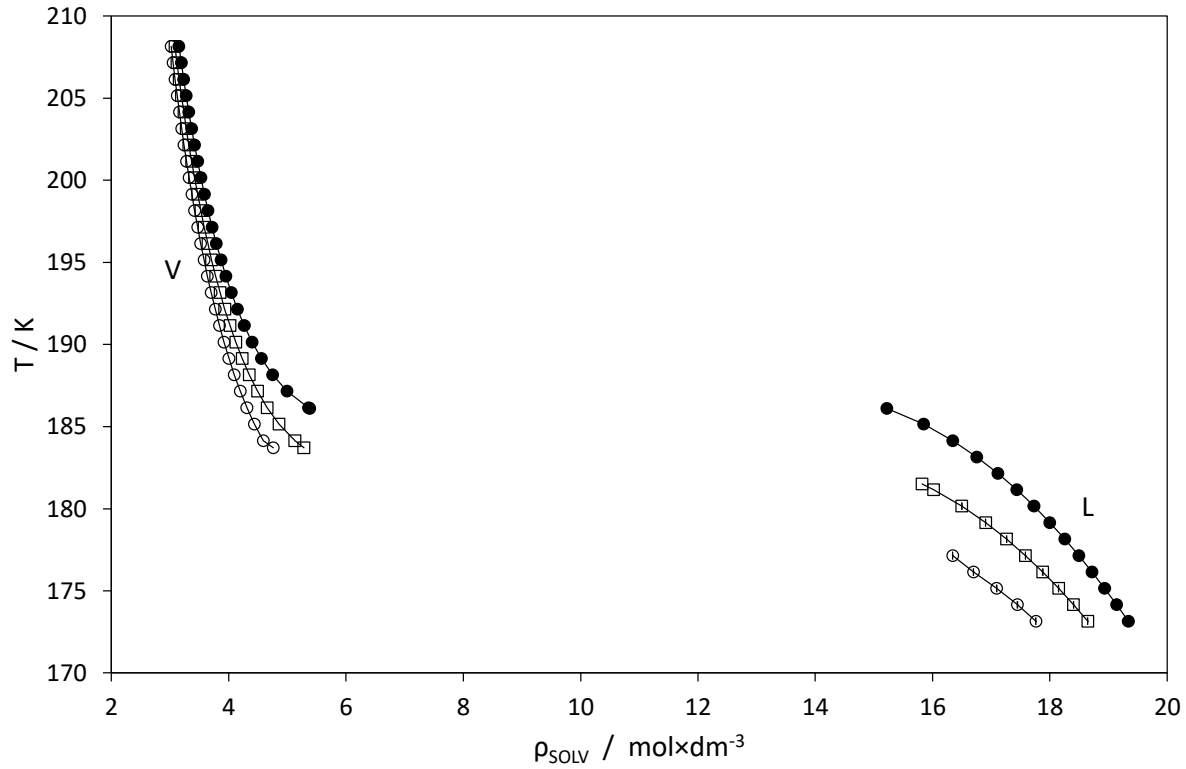

Fig. 9. Molar density of the solvents A (●), B (□) and C (○) at 4 MPa as a function of temperature.

In the temperature range considered in this study, the second effect related to the addition of nitrogen to the solvent is the modification of the temperature ranges interested by the SVE, SLVE, and SLE, as shown also in the modeling section.

Indeed, increasing N_2-content in the solvent (nitrogen + methane mixture) makes the SVE exist at lower temperatures with respect to the methane + carbon dioxide system. To illustrate, Fig. 7 shows that the SVE has been measured down to 190.406 K for the solvent A (point n°12 in Table 4), down to 188.509 K for the solvent B (point n°39 in Table 7), and down to 184.521 K for the solvent C (point n°57 in Table 9).

The measurement of the SVE at lower temperatures passing from solvent A to solvent C has been possible seeing that the temperature range interested by the SLVE occurs at lower

temperatures for increasing N_2-content in the solvent. As a result, the addition of nitrogen makes the SLE appear at lower temperatures for the solvents B and C with respect to the methane + carbon dioxide system. To illustrate, Fig. 8 shows that the SLE has been measured starting at 189.643 K for solvent A (point n°26 in Table 6), 182.565 K for solvent B (point n°40 in Table 8), and 178.765 K for solvent C (point n°58 in Table 10).

Table 11. VLE data measured for the (1) nitrogen + (2) methane + (3) carbon dioxide system using the solvents B and C.

Point	T [K]	P [MPa]	U(x_1)	x_2	U(x_2)	x_3	U(x_3)	U(y_1)	y_2	U(y_2)	y_3	U(y_3)
63	183.532	4.003	0.0026	0.8956	0.0044	0.0552	0.0023	0.0049	0.8713	0.0054	0.0232	0.0008
64	182.545	4.001	0.0041	0.8921	0.0068	0.0504	0.0030	0.0055	0.8599	0.0059	0.0202	0.0007
65	182.542	3.998	0.0025	0.9110	0.0035	0.0369	0.0014	0.0050	0.8761	0.0053	0.0158	0.0006
66	181.561	4.000	0.0039	0.8917	0.0056	0.0448	0.0023	0.0062	0.8467	0.0065	0.0179	0.0006
67	181.557	3.996	0.0035	0.9129	0.0047	0.0283	0.0014	0.0058	0.8676	0.0060	0.0123	0.0005
68	181.554	4.002	0.0027	0.9277	0.0031	0.0173	0.0007	0.0058	0.8807	0.0060	0.0079	0.0003
69	180.623	4.007	0.0046	0.8854	0.0063	0.0414	0.0023	0.0069	0.8310	0.0072	0.0163	0.0005
70	180.571	4.003	0.0031	0.9201	0.0035	0.0156	0.0006	0.0067	0.8631	0.0068	0.0070	0.0003
71	180.275	4.001	0.0042	0.9111	0.0049	0.0198	0.0010	0.0069	0.8519	0.0071	0.0086	0.0003
72	179.634	3.998	0.0044	0.8818	0.0058	0.0367	0.0023	0.0076	0.8170	0.0078	0.0148	0.0005
73	179.589	3.998	0.0035	0.9091	0.0040	0.0167	0.0006	0.0073	0.8431	0.0075	0.0072	0.0003
74	179.589	4.010	0.0036	0.9117	0.0040	0.0137	0.0005	0.0077	0.8447	0.0078	0.0061	0.0002
75	179.145	4.003	0.0044	0.8776	0.0054	0.0364	0.0014	0.0077	0.8092	0.0079	0.0142	0.0005
76	179.092	4.000	0.0040	0.9081	0.0043	0.0133	0.0005	0.0081	0.8367	0.0082	0.0058	0.0002
77	178.602	4.006	0.0041	0.9035	0.0045	0.0127	0.0005	0.0086	0.8272	0.0087	0.0055	0.0002

U(T) = 0.004 K; U(P) = 0.002 MPa

Table 12. SLVE data measured for the (1) nitrogen + (2) methane + (3) carbon dioxide system using the solvents B and C.

Point	T [K]	P [MPa]	U(x_1)]	x_2	U(x_2)	x_3	U(x_3)	U(y_1)	y_2	U(y_2)	y_3	U(y_3)
78[1]	183.560	4.002						0.0049	0.8646	0.0053	0.0247	0.0008
79[1]	183.537	4.040						0.0050	0.8620	0.0055	0.0246	0.0008
80[1]	183.521	4.014						0.0049	0.8622	0.0053	0.0246	0.0008
81[1]	182.571	3.998						0.0055	0.8504	0.0059	0.0229	0.0007
82	182.533	4.025	0.0035	0.8795	0.0059	0.0585	0.0030	0.0056	0.8471	0.0060	0.0227	0.0007
83	181.540	4.000	0.0031	0.8760	0.0044	0.0553	0.0019	0.0061	0.8344	0.0065	0.0212	0.0007
84	181.521	4.006	0.0038	0.8757	0.0054	0.0554	0.0044	0.0063	0.8330	0.0067	0.0210	0.0007
85[1]	181.055	4.003						0.0068	0.8264	0.0071	0.0203	0.0007
86	181.039	3.997	0.0033	0.8736	0.0045	0.0535	0.0018	0.0065	0.8266	0.0069	0.0203	0.0006
87	180.541	3.998	0.0034	0.8710	0.0046	0.0518	0.0017	0.0069	0.8187	0.0072	0.0195	0.0006
88[1]	180.058	3.998						0.0074	0.8109	0.0077	0.0188	0.0006
89	180.043	3.998	0.0036	0.8682	0.0048	0.0502	0.0017	0.0075	0.8106	0.0077	0.0188	0.0006

[1] Because of the global composition of the mixture, the amount of the liquid phase within the equilibrium cell was not enough developed to be sampled by the liquid ROLSI® sampler.
U(T) = 0.004 K; U(P) = 0.002 MPa

5. Comparison with modeling results

The thermodynamic package used in this work has been obtained coupling a common fluid phase model and the well-known classical approach for solid carbon dioxide; the isofugacity condition at SVE, SLE, or SLVE has been solved under the assumption that the solid phase is made by the pure solid former, as deeply illustrated by Campestrini et al [47].

The Peng-Robinson (PR) EoS [11] as implemented in Aspen HYSYS® V10 [12] has been selected for calculating the partial molar fugacity of N_2, CH_4, and CO_2 in the liquid and vapor phases. This fluid phase model involves the acentric factor-dependent alpha function [11] and the Van der Waals one-fluid mixing rules for the calculation of the well-known parameters a and b of cubic EoSs. As a consequence, the only parameters needed for the application of the PR EoS were the critical pressure (P_C), the critical temperature (T_C), and acentric factor (ω) of the pure fluids of interest in this work (nitrogen, methane, and carbon dioxide), and the binary interaction parameters (k_{ij}) of the corresponding binary mixtures (nitrogen + methane, nitrogen + carbon dioxide, and methane + carbon dioxide). For all these parameters, values have been taken from Aspen HYSYS® V10 database and are given in Table 13.

When applied at temperatures lower than the triple-point temperature of a pure fluid *i*, the classical approach relates its fugacity in the solid phase ($f_i^{0,S}$) to its fugacity in the subcooled liquid state ($f_i^{0,L}$) and to its latent heat of melting ($\Delta H_m = H_L - H_S$), specific heat change upon melting ($\Delta Cp_m = Cp_L - Cp_S$), and its molar volume change upon melting ($\Delta v_m = v_L - v_S$) [13].

$$\ln\frac{f_i^{0,S}(T,P)}{f_i^{0,L}(T,P)} = \frac{\Delta H_m}{RT_{T,i}}\left(1-\frac{T_{T,i}}{T}\right)+\frac{\Delta Cp_m}{R}\left(\frac{T_{T,i}}{T}-1-\ln\frac{T_{T,i}}{T}\right)-\frac{\Delta v_m}{RT}\left(P-P_{T,i}\right) \qquad (1)$$

Except the system temperature T and pressure P, all the properties within Eq. (1) are triple point properties ($T_{T,i}$ and $P_{T,i}$ are the triple-point temperature and pressure of component *i*, respectively). As a consequence, it should be remembered that constant values of ΔH_m, ΔCp_m, and Δv_m have been adopted in the modeling work, and these values are equal to the values at the triple-point of the fluid. Table 14 summarizes the triple-point properties used in this work for carbon dioxide, corresponding to experimental values taken from the DIPPR database [48].

Table 13: Critical-point properties and acentric factors of N_2, CH_4, and CO_2, and binary interaction parameters of the corresponding binary mixtures [12].

Pure Fluids			
Fluid	**T_C [K]**	**P_C [MPa]**	**Ω**
N_2	126.194	3.39437	0.04
CH_4	190.699	4.64068	0.0115
CO_2	304.100	7.37	0.2389
Binary Mixtures			
Mixture		**k_{ij}**	
N_2 + CH_4		0.036	
N_2 + CO_2		-0.02	
CH_4 + CO_2		0.1	

Table 14: Triple-point properties of CO_2 used in this work [48].

Fluid	**T_T [K]**	**P_T [MPa]**	**ΔH_m [kJ/mol]**	**ΔCp_m [kJ/mol/K]**	**Δv_m [dm^3/mol]**
CO_2	216.592	0.49952	8.65	0.0138	0.00858

In the following, experimental measurements are qualitatively compared with the calculated phase behaviors.

All the VLE measurements gathered in Table 5 are compared to the calculated phase equilibrium behavior at 4 MPa in Fig. 10. In Fig. 10, the x-axis representing the molar fraction of carbon dioxide has been limited to a CO_2-content of 11%. The horizontal line represents the calculated SLVE condition of the mixture at 4 MPa, whereas symbols are the values measured between 3.969 MPa and 4.031 MPa.

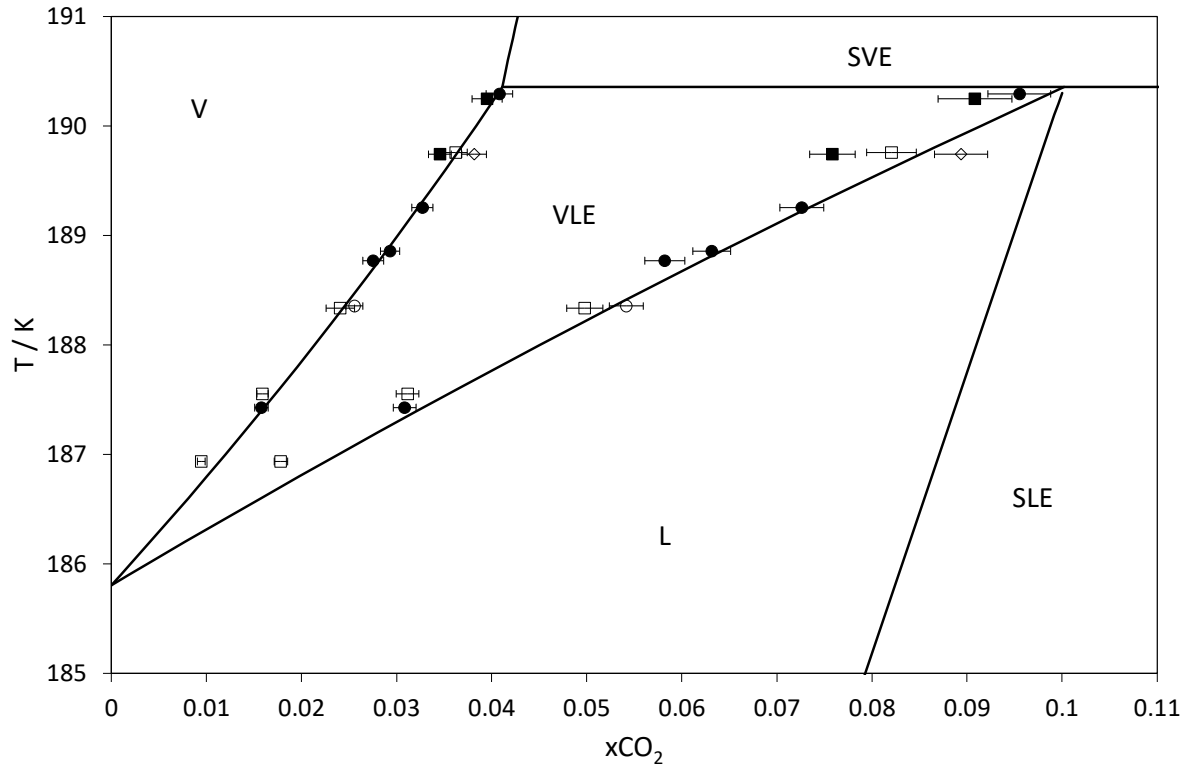

Fig. 10. VLE measurements and calculated phase equilibrium behavior of the CH_4 + CO_2 system at 4 MPa from 185 K up to 191 K for CO_2-contents lower than 11%.
Experimental values: ■ : points n°14 (4.015 MPa) and n°17 (4.031 MPa); □ : points n°15, n°22, n°23, and n°25 at about 4.00 MPa; ● : points n°13, n°18, n°19, n°20, and n°24 at about 3.99 MPa; ○ : point n°21 at 3.977 MPa; ◊ : point n°16 at 3.969 MPa. Calculated values: – .

According to the experimental points shown in Fig. 10 (filled squares at 4.015 and 4.031 MPa, open squares at about 4.00 MPa, filled points at about 3.99 MPa, open point at 3.977 MPa, and open diamond at 3.969 MPa), a pressure increase at a certain temperature provokes a decrease of the CO_2-content in the equilibrium phases at VLE. This decrease is more pronounced in the liquid

than in the vapor phase owing to the fact that, in the pressure-composition diagram, the slope of the liquid curve is lower than that of the vapor when the global composition of the mixture approaches pure methane, as pointed out by the modeling (and experimental) results illustrated in Fig. 11.

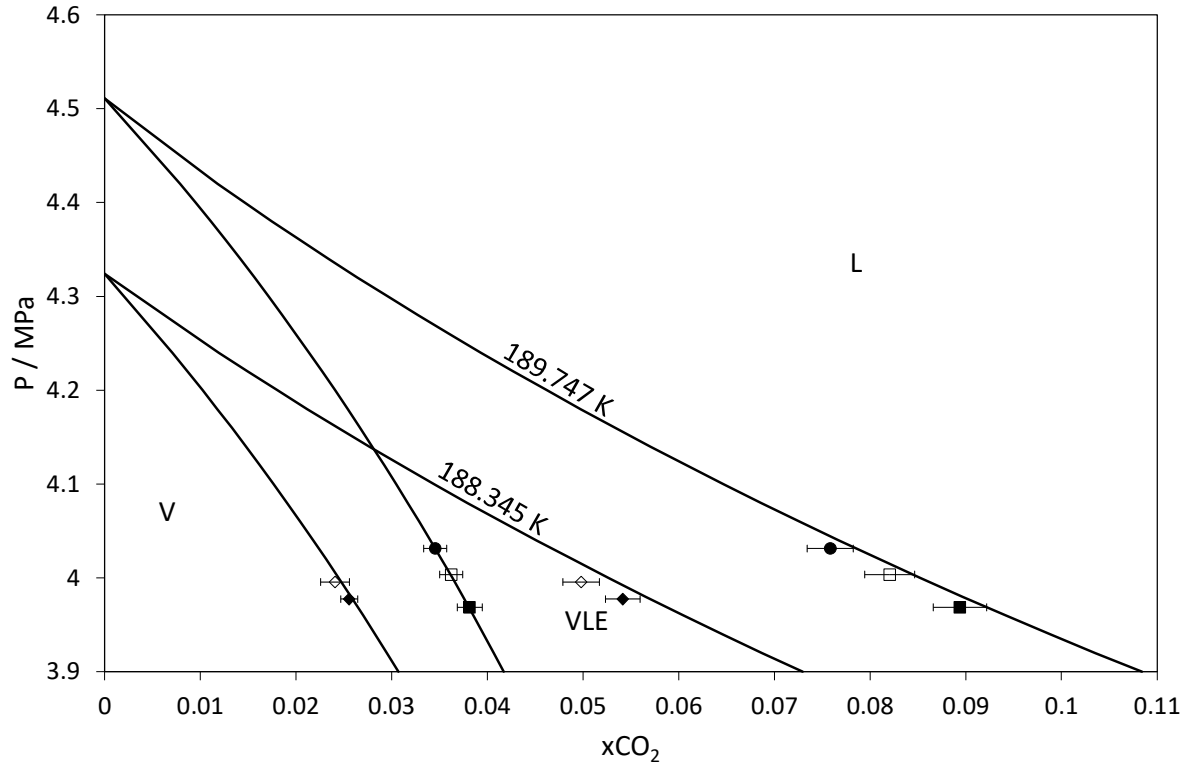

Fig. 11. Experimental and calculated phase equilibrium behavior of the CH_4+CO_2 system at 188.345 K and 189.747 K from 3.9 MPa up to 4.6 MPa for CO_2-contents lower than 11%. Experimental values at 189.747 K (average value): ● : point n°17 at 4.031 MPa; □ : point n°15 at 4.004 MPa; ■ : point n°16 at 3.969 MPa. Experimental values at 188.345 K (average value): ◊ : point n°22 at 3.996 MPa; ♦ : point n°21 at 3.977 MPa. Calculated values: – .

The solubilities of solid carbon dioxide in vapor and liquid solvent A tabulated in Tables 4 and 6 are qualitatively compared to modeling results in Fig. 12, where the calculated VLE has been omitted. The calculated SLVE temperature is about 190.3 K.

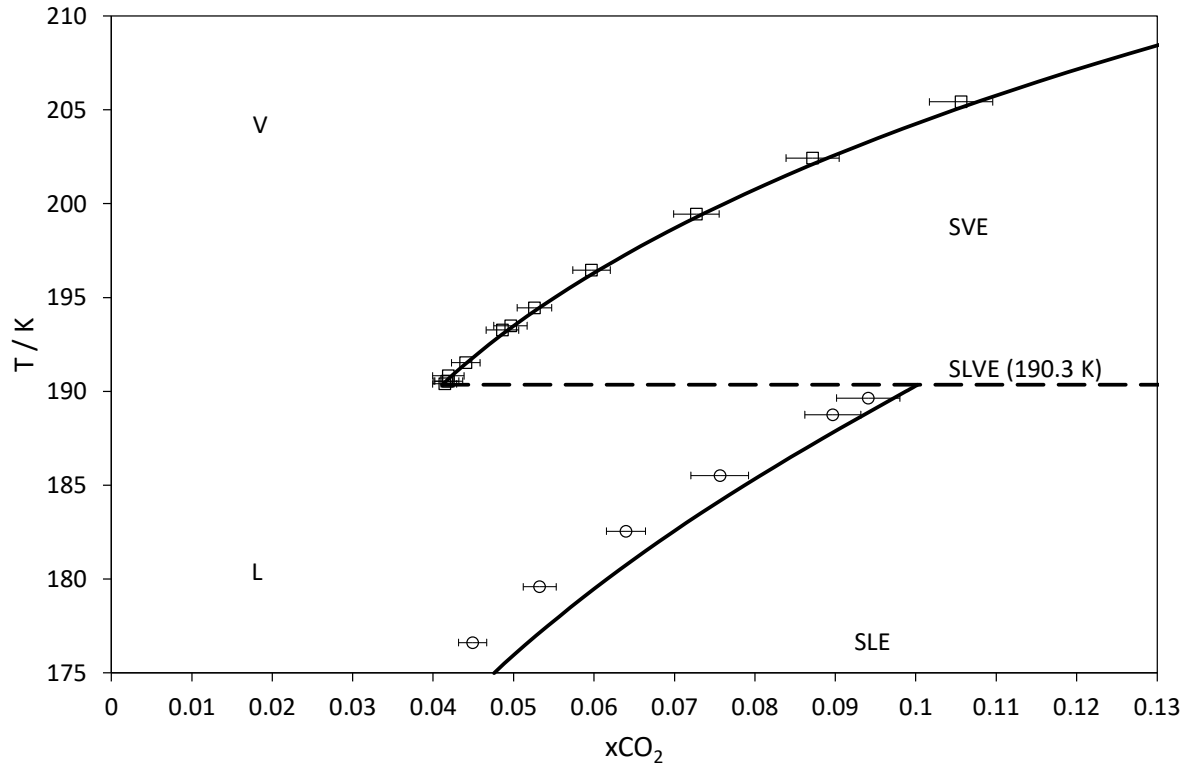

Fig. 12. Calculated and experimental CO_2 compositions at SVE and SLE for the solvent A + carbon dioxide system.
Experimental values: vapor phase (□); liquid phase (○). Calculated values: SVE and SLE (–), SLVE (– –).

The solubilities of solid carbon dioxide in vapor and liquid solvent B tabulated in Tables 7 and 8 are qualitatively compared to modeling results in Fig. 13; calculated VLE and SLVE have been omitted, thus the SVE runs down to the upper SLVE temperature (about 187.3 K), whereas the SLE starts at the lower SLVE temperature (about 184.4 K).

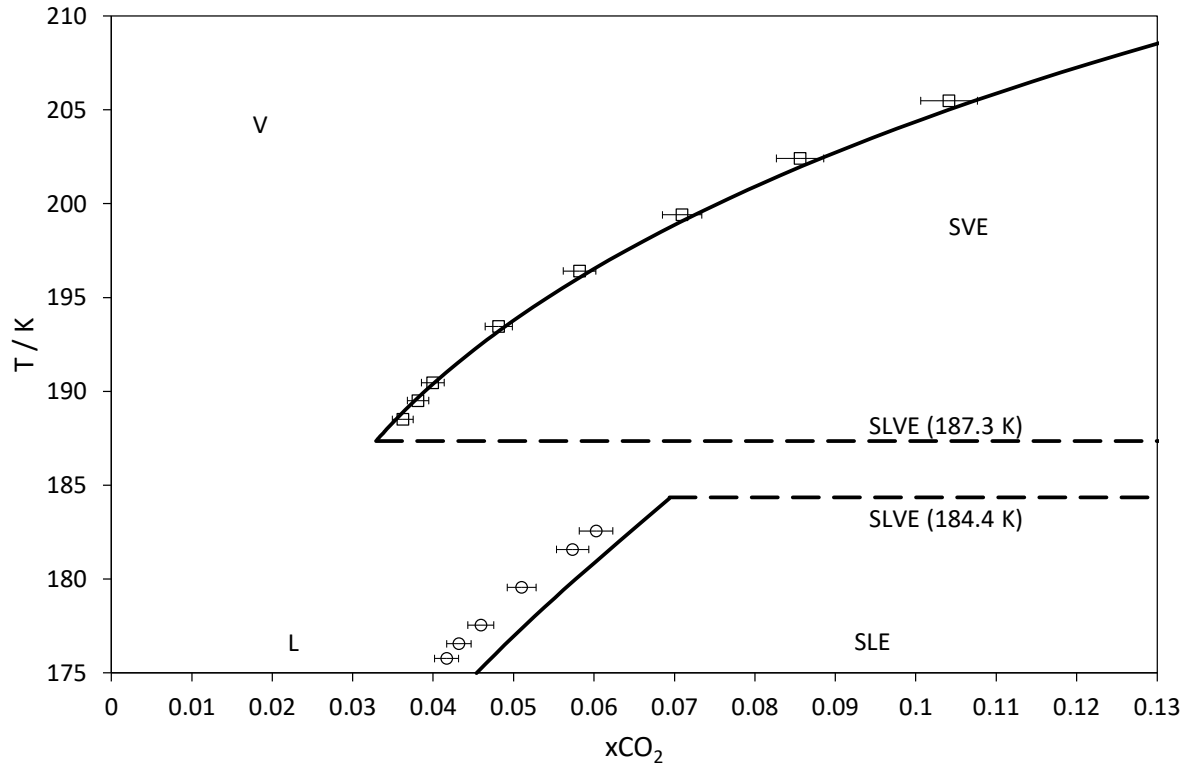

Fig. 13. Calculated and experimental CO_2 compositions at SVE and SLE for the solvent B + carbon dioxide system.
Experimental values: vapor phase (□); liquid phase (○). Calculated values: SVE and SLE (–), SLVE (– –).

The solubilities of solid carbon dioxide in vapor and liquid solvent C tabulated in Tables 9 and 10 are qualitatively compared to modeling results in Fig. 14; calculated VLE and SLVE have been omitted, thus the SVE runs down to the upper SLVE temperature (about 184.5 K), whereas the SLE starts at the lower SLVE temperature (about 178.9 K).

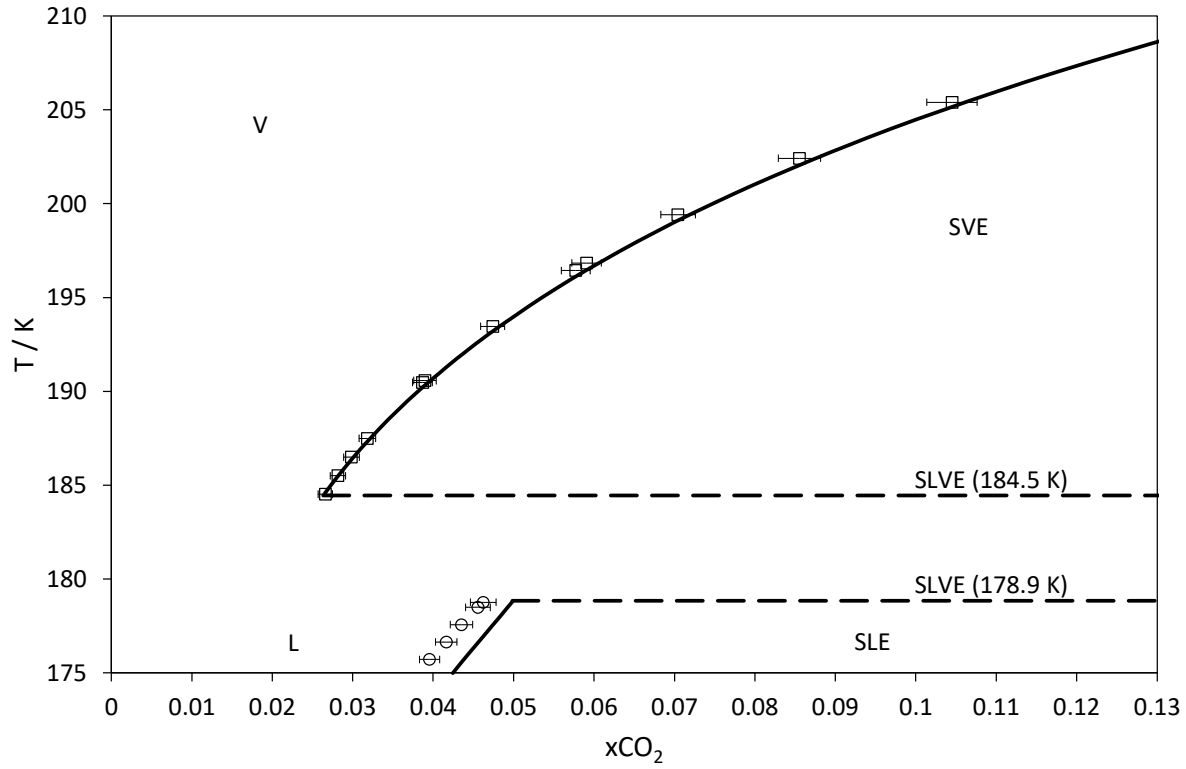

Fig. 14. Calculated and experimental CO_2 compositions at SVE and SLE for the solvent C + carbon dioxide system.
Experimental values: vapor phase (□); liquid phase (○). Calculated values: SVE and SLE (–), SLVE (– –).

In Figs. 12 – 14, it is possible to observe that the agreement between experimental and calculated solubilities is better in the vapor phase than in the liquid phase. It follows that for a given composition of CO_2, the SVE temperature calculated by the model is close to the experimental value, whereas the calculated SLE temperature is lower than the experimental value. As a consequence, the solid appearance temperature of a liquid mixture of known global composition is underestimated by the model. At the same time, at a given temperature, the model overestimates the solubility of CO_2 with respect to the value that can be inferred from the experimental values more at SLE than at SVE.

This deviation between modeling and experimental results can be related, at least for the Solvent A + carbon dioxide system to an improper value used for the binary interaction parameter of the CH_4 + CO_2 system, seeing that the experimental solubilities of solid carbon dioxide in liquid methane presented in this work are in a rather good quantitative agreement with the collected literature values, as pointed out in Fig. 6.

Some of the experimental SVE, SLE, VLE, and SLVE gathered in Tables 4 – 12 are qualitatively compared to modeling results in the following ternary diagram. Figs. 15 – 19 show the phase equilibrium behavior of the ternary nitrogen + methane + carbon dioxide system in the methane-rich region.

Modeling results (VLE, SVE, SLE, and SLVE) calculated at the average pressures and temperatures of a certain number of experimental points are represented by solid lines.

Experimental results are represented by symbols: open symbols correspond to VLE, SLE, and SVE values of the solvent A + carbon dioxide system, open squares are related to SLE and SVE values of the solvent B + carbon dioxide system, open triangles correspond to SLE and SVE values of the solvent C + carbon dioxide system. Full squares and full circles are used for the compositions of vapor and liquid phases of the ternary system at SLVE and VLE, respectively.

Finally, dotted lines represent the locus of the global composition having a constant ratio between the molar fractions of nitrogen and methane (5%N_2 + 95%CH_4 for solvent B, 10%N_2 + 90%CH_4 for solvent C).

Fig. 15 presents the comparison between calculated and experimental values (points n°11 in Table 4, n°37 in Table 7, and n°53 in Table 9) at average temperature and pressure of 190.495 K and 4.007 MPa, respectively.

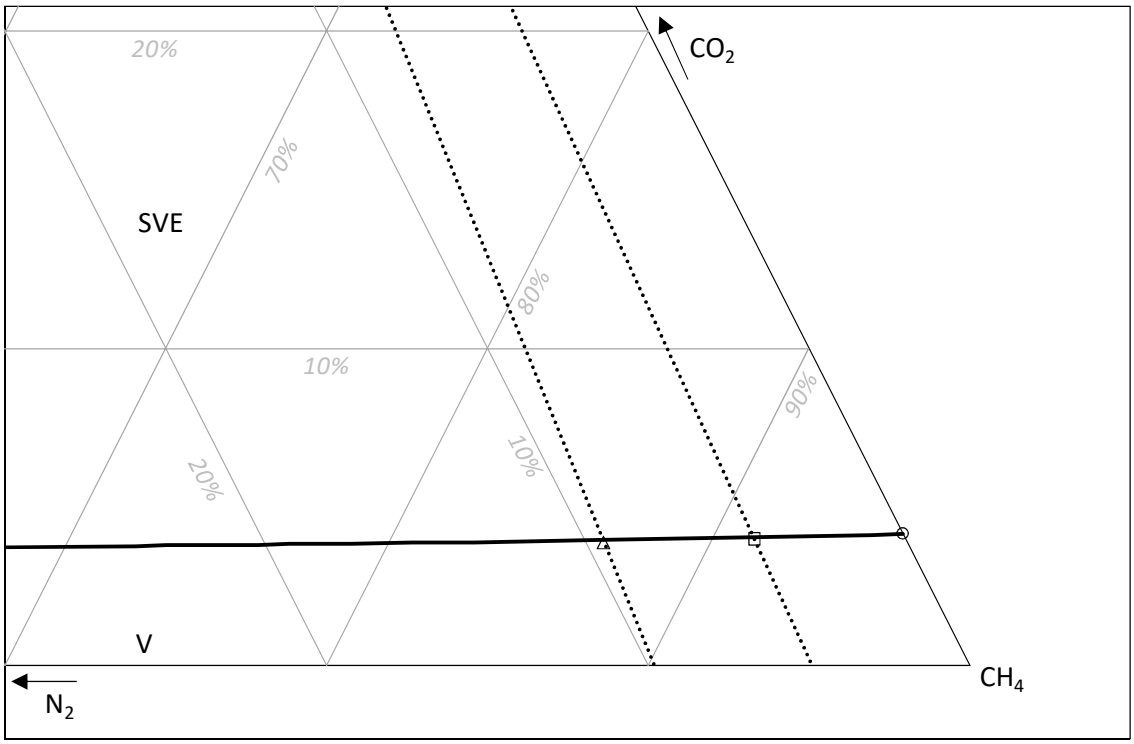

Fig. 15. Zoom in the CH_4-rich region of the ternary diagram of the N_2 + CH_4 + CO_2 system at average temperature (190.495 K) and pressure (4.007 MPa) of points n°11, n°37, and n°53. Experimental values: point n°11, solvent A (○); point n°37, solvent B (□); point n°53, solvent C (Δ). Solid lines are modeling results, dotted lines refer to N_2/CH_4 ratios of solvents B and C.

Fig. 16 presents the comparison between calculated and experimental values (points n°23 in Table 5, and n°54 in Table 9) at average temperature and pressure of 187.525 K and 4.000 MPa, respectively.

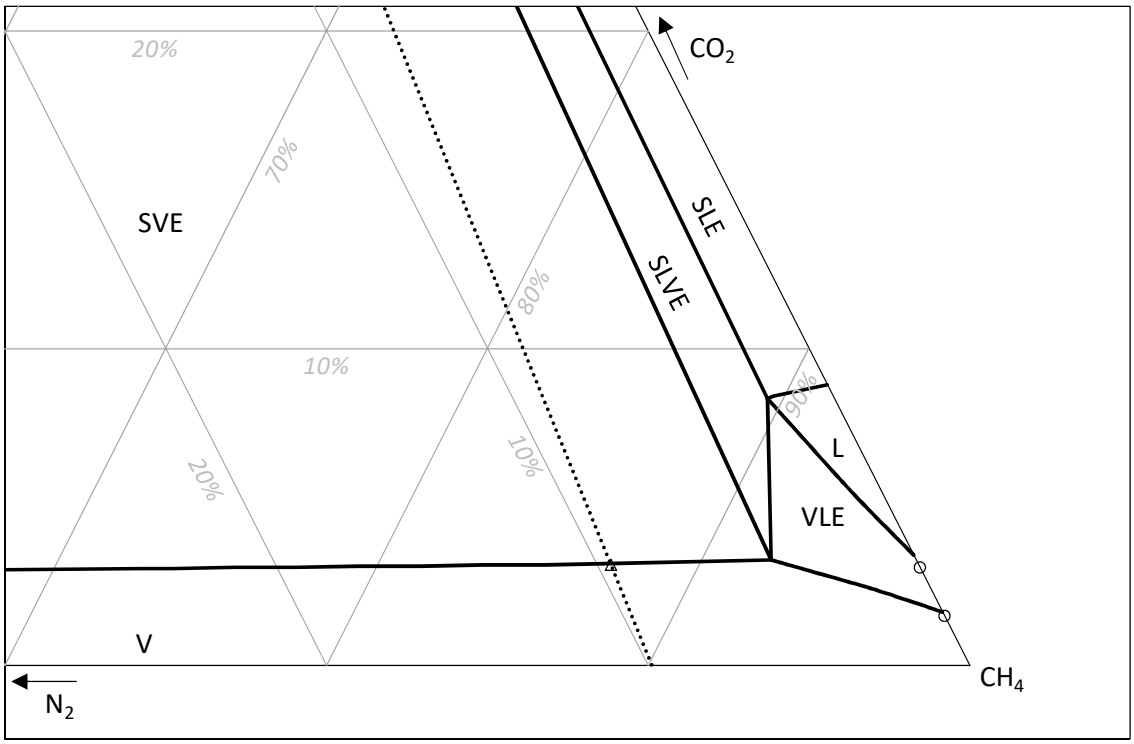

Fig. 16. Zoom in the CH_4-rich region of the ternary diagram of the N_2 + CH_4 + CO_2 system at average temperature (187.525 K) and pressure (4.000 MPa) of points n°23 and n°54.
Experimental values: point n°23, solvent A (○); point n°54, solvent C (Δ). Solid lines are modeling results, dotted line refers to N_2/CH_4 ratio of solvent C.

Fig. 17 presents the comparison between calculated and experimental values (points n°29 in Table 6, n°40 in Table 8, n°64 and n°65 in Table 11, and n°82 in Table 12) at average temperature and pressure of 182.548 K and 4.004 MPa, respectively.

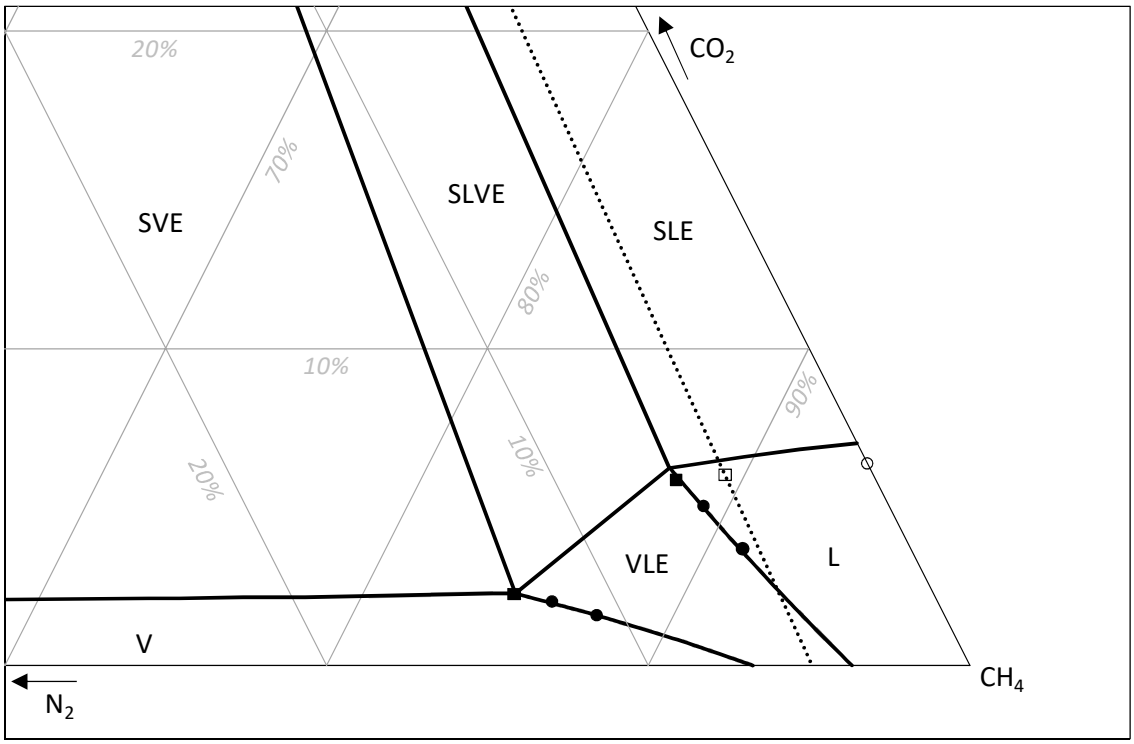

Fig. 17. Zoom in the CH_4-rich region of the ternary diagram of the N_2 + CH_4 + CO_2 system at average temperature (182.548 K) and pressure (4.004 MPa) of points n°29, n°40, n°64, n°65, and n°82.
Experimental values: point n°29, solvent A (○); point n°40, solvent B (□); points n°64 and n°65 (●); point n° 82 (■). Solid lines are modeling results, dotted lines refer to N_2/CH_4 ratio of solvent B.

Fig. 18 presents the comparison between calculated and experimental values (points n°41 in Table 8, n°66-n°68 in Table 11, and n°84 in Table 12) at average temperature and pressure of 181.554 K and 4.001 MPa, respectively.

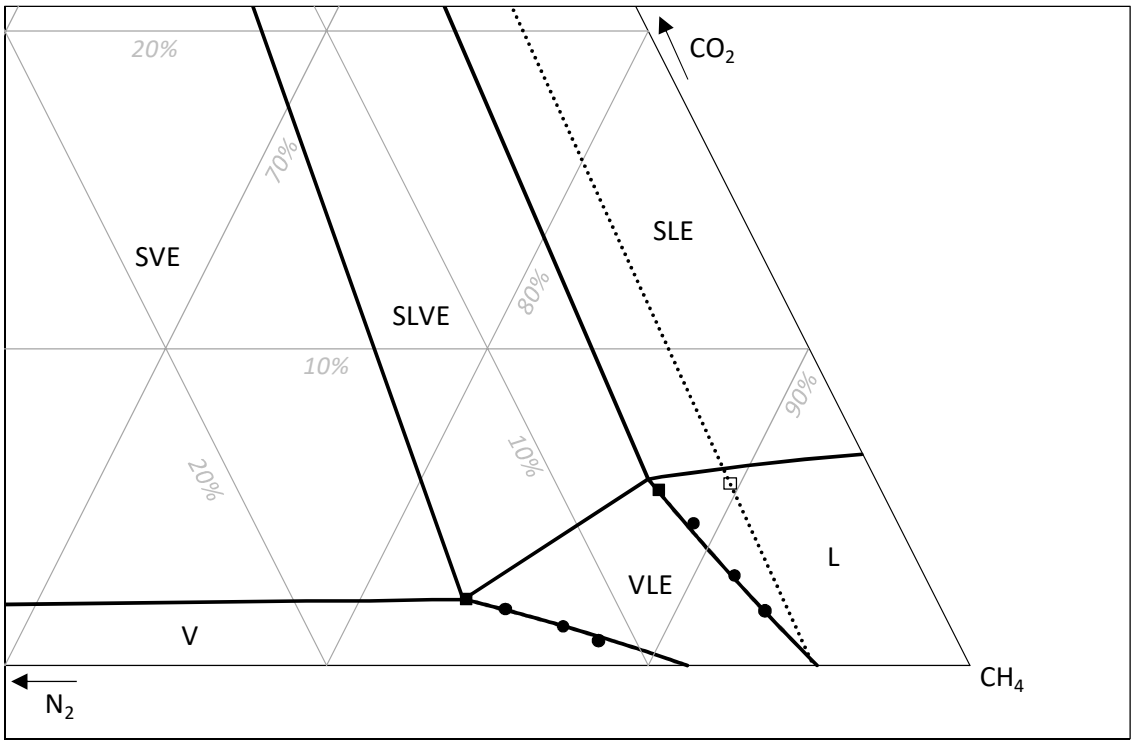

Fig. 18. Zoom in the CH_4-rich region of the ternary diagram of the N_2 + CH_4 + CO_2 system at average temperature (181.554 K) and pressure (4.001 MPa) of points n°41, n°66, n°67, n°68, and n°84.
Experimental values: point n°41, solvent B (□); points n°66-n°68 (●); point n° 84 (■). Solid lines are modeling results, dotted line refers to N_2/CH_4 ratio of solvent B.

Fig. 19 presents the comparison between calculated and experimental values (points n°31 in Table 6, n°44 in Table 8, and n°61 in Table 10) at average temperature and pressure of at 176.607 K and 3.976 MPa.

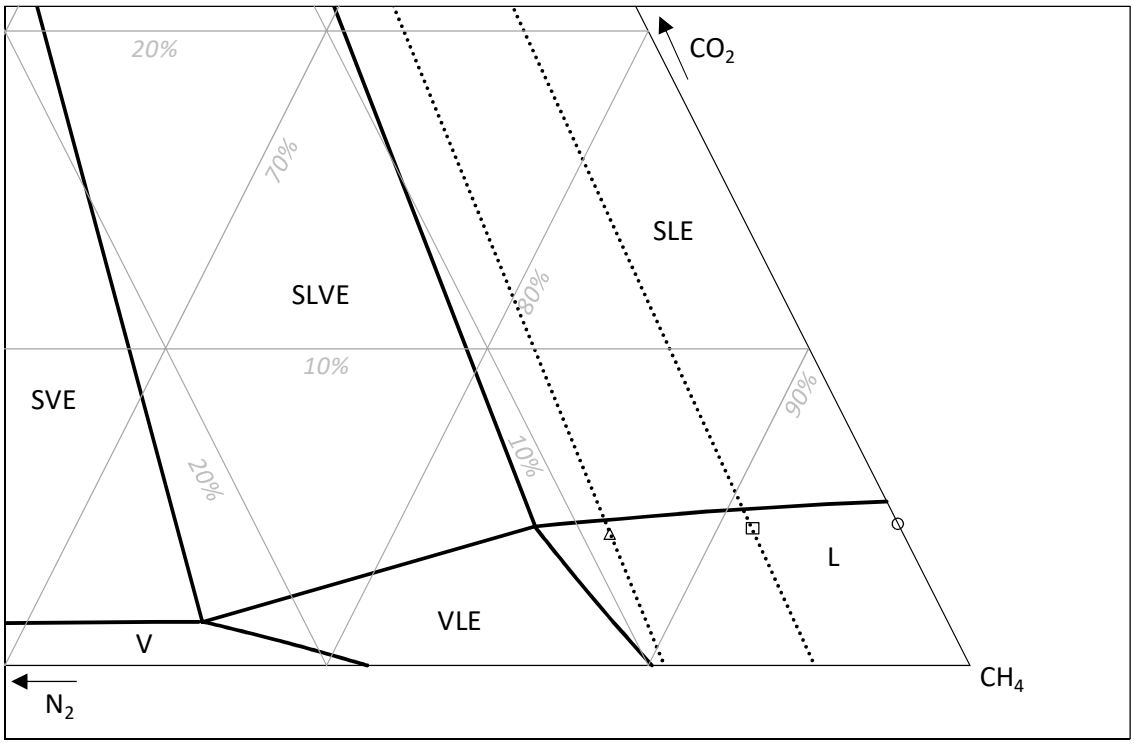

Fig. 19. Zoom in the CH_4-rich region of the ternary diagram of the N_2 + CH_4 + CO_2 system at average temperature (176.607 K) and pressure (3.976 MPa) of points n°31, n°44, and n°61. Experimental values: point n°31, solvent A (○); point n°44, solvent B (□); point n°61, solvent C (Δ). Solid lines are modeling results, dotted lines refer to N_2/CH_4 ratios of solvents B and C.

By observing Figs. 15 – 19, the evolution for decreasing temperatures of the phase equilibrium behavior of the nitrogen + methane + carbon dioxide system at a nominal pressure of 4 MPa can be drawn.

At temperatures higher than the saturation temperature of methane at 4.00 MPa (T_{SAT} = 185.841 K [29]), the nitrogen + methane system is in the vapor/supercritical state, as in Fig. 15. Solid carbon dioxide can be at equilibrium only with this vapor/supercritical phase.

The only liquid phase that can appear in the ternary diagram at temperatures higher than T_{SAT} develops from the right edge of the diagram, the one representing the phase equilibrium behavior of the methane + carbon dioxide system, as in Fig. 16. In Fig. 16, a SLVE and a VLE then appear due to the presence of this liquid phase, and solid carbon dioxide can be at equilibrium with a liquid phase, or a vapor phase richer in nitrogen than the liquid phase, or both (at SLVE), according to the global composition of the mixture.

As the temperature drops below T_{SAT}, pure methane is stable as a liquid and the VLE and SLVE move from the right to the left of the ternary diagram towards compositions richer in nitrogen. A VLE exists then for the nitrogen + methane mixture, whereas the methane + carbon dioxide mixture is at SLE, as in Fig. 17.

This repositioning of the SLVE triangle in the direction of nitrogen related to the change of position of the VLE of the nitrogen + methane mixture proceeds for decreasing temperatures as illustrated in Figs. 18 and 19.

It is interesting to notice that cooling the system temperature from about 187 K (Fig. 16) down to about 177 K (Fig. 19) through T_{SAT} entails not only the repositioning of the SLVE triangle from the right to the left of the ternary diagram, but also the thickening or expansion of the surface of the SLVE triangle. Remembering that, at a certain temperature and pressure, all the global compositions of the mixture falling within the SLVE triangle lead to the SLVE, the expansion of the surface of the SLVE triangle with decreasing temperatures means that a larger number of global compositions of the ternary mixture leads to SLVE at about 177 K (Fig. 19) than at 187 K (Fig. 16).

The experimental values tabulated in Tables 4 – 12 have been quantitatively compared with modeling results. For all the 89 experimental points (28 VLE, 32 SVE, 17 SLE, and 12 SLVE), the thermodynamic package has been applied at constant temperature and pressure (equal to the experimental values) to calculate the equilibrium compositions successively compared with experimental values. Common statistical indexes (AAD, Bias, and MAD) have been used for the comparison; please refer to the Supporting Material for details related to the calculation of the statistical indexes.

A common FLASH calculation at given global composition of the mixture (CH_4 + CO_2 or N_2 + CH_4 + CO_2) has then been carried out for all the VLE data.

A "FLASH" calculation has been carried out for the equilibria involving solid carbon dioxide. For SVE (SLE) data, the CO_2 composition of the vapor (liquid) phase at equilibrium with solid carbon dioxide rather than the global composition of the mixture has been given as input value and iterated until satisfying the isofugacity condition between the fugacity of pure carbon dioxide in the solid phase from Eq. (1) and its partial molar fugacity in the vapor (liquid) phase from the PR EoS. During the iteration, the compositions of nitrogen and methane in the fluid phase at equilibrium with solid carbon dioxide have been calculated assuming that the ratio between their molar fractions is equal to the concentrations of the three solvents A, B, and C.

For SLVE data, a common FLASH calculation has been performed at given global composition and the partial molar fugacity of carbon dioxide in the vapor phase (equal to that of the liquid) has been compared to the fugacity of solid carbon dioxide. The global composition has then been iterated until satisfying the SLVE condition.

The quantitative comparison between experimental and calculated VLE and SLVE data is gathered in Table 15.

Table 15: Quantitative comparison between VLE and SLVE data and modeling results for the (1)N_2 + (2)CH_4 + (3)CO_2 mixtures.

Equilibrium	**VLE**		**SLVE**
Mixture	**CH_4 + CO_2**	**N_2 + CH_4 + CO_2**	**N_2 + CH_4 + CO_2**
AAD(x_1)%		1.87	2.72
Bias(x_1)%		1.87	2.72
MAD(x_1)%		3.61	3.40
AAD(x_2)%	0.39	0.22	0.62
Bias(x_2)%	-0.39	-0.22	-0.62
MAD(x_2)%	0.61	0.31	0.65
AAD(x_3)%	7.95	2.90	6.45
Bias(x_3)%	7.95	2.90	6.45
MAD(x_3)%	27.23	4.77	7.01
AAD(y_1)%		1.83	1.84
Bias(y_1)%		-1.83	1.84
MAD(y_1)%		3.81	4.26
AAD(y_2)%	0.06	0.35	0.28
Bias(y_2)%	-0.05	0.35	-0.28
MAD(y_2)%	0.20	0.49	0.56
AAD(y_3)%	3.59	4.07	0.82
Bias(y_3)%	3.51	-4.07	-0.80
MAD(y_3)%	20.94	6.70	1.54

With respect to VLE data of the CH_4 + CO_2 system, deviations up to about 30% and 20% are encountered for the composition of carbon dioxide in the liquid and vapor phase, respectively, whereas the deviations related to methane are lower than 1% (see 2nd column of Table 15). The high deviations for carbon dioxide at VLE are due to the low concentration of this component in the mixture when approaching the saturation temperature of methane; the lowest experimental CO_2

molar fraction in the liquid and vapor phases are 1.78% and 0.95%, respectively (point n°25 in Table 5).

For VLE data of the N_2 + CH_4 + CO_2 system, deviations are lower than 4%, 0.5%, and 7% for methane, nitrogen, and carbon dioxide, respectively (see 3rd column of Table 15). For SLVE data, deviations are lower than 5%, 1%, and 7% for methane, nitrogen, and carbon dioxide, respectively (see 4th column of Table 15). All these deviations are within the experimental uncertainties.

The quantitative comparison between experimental and calculated SVE and SLE data is gathered in Table 16.

For the solvent A, the deviations given in Table 16 are of about 0.2% and 2% for the CH_4-composition and CO_2-composition, respectively, in the vapor phase at SVE (2nd column). These values are within the experimental uncertainties (a maximum value of 0.4% and 6.2% for CH_4 and CO_2, respectively). Deviations are of about 0.8% and 15% for the CH_4-composition and CO_2-composition in the liquid phase at SLE (5th column), respectively.

For the solvent B, the deviations given in Table 16 are of about 3%, 0.5%, and 3% for the N_2-composition, CH_4-composition, and CO_2-composition, respectively, in the vapor phase at SVE (3rd column). These values are within the experimental uncertainties (a maximum value of 4.8%, 0.6% and 3.5% for N_2, CH_4, and CO_2, respectively). Deviations are of about 4%, 1%, and 14% for the N_2-composition, CH_4-composition, and CO_2-composition, respectively, in the liquid phase at SLE (6th column). These values are similar to the experimental uncertainties only for nitrogen (maximum of 4.8%) and methane (maximum of 0.4%), but much higher for carbon dioxide (maximum of 4%).

For the solvent C, the deviations given in Table 16 are of about 2%, 0.5%, and 3% for the N_2-composition, CH_4-composition, and CO_2-composition, respectively, in the vapor phase at SVE (4th column). These values are similar to the experimental uncertainties (a maximum value of 4.7%, 0.7% and 3.6% for N_2, CH_4, and CO_2, respectively). Deviations are of about 5%, 2%, and 34% for the N_2-composition, CH_4-composition, and CO_2-composition, respectively, in the liquid phase at SLE (7th column). These values are similar to the experimental uncertainties only for nitrogen (maximum of 5.0%) and methane (maximum of 0.6%), but much higher for carbon dioxide (maximum of 3.4%).

Table 16: Quantitative comparison between SVE and SLE data and modeling results for the (1)N_2 + (2)CH_4 + (3)CO_2 mixtures.

Equilibrium		**SVE**			**SLE**	
Solvent	**A**	**B**	**C**	**A**	**B**	**C**
AAD(x_1)%					2.65	4.06
Bias(x_1)%					2.65	4.06
MAD(x_1)%					3.60	4.39
AAD(x_2)%				0.56	0.71	1.55
Bias(x_2)%				-0.56	-0.71	-1.55
MAD(x_2)%				0.75	0.82	2.11
AAD(x_3)%				8.60	10.82	22.71
Bias(x_3)%				8.60	10.82	22.71
MAD(x_3)%				15.09	13.50	34.10
AAD(y_1)%		2.31	1.44			
Bias(y_1)%		2.31	1.44			
MAD(y_1)%		2.69	1.92			
AAD(y_2)%	0.08	0.24	0.26			
Bias(y_2)%	-0.07	-0.24	-0.26			
MAD(y_2)%	0.23	0.48	0.44			
AAD(y_3)%	1.05	2.03	1.56			
Bias(y_3)%	0.92	1.20	1.48			
MAD(y_3)%	2.17	3.04	2.59			

The higher deviations between modeling and experimental results obtained for SLE data with respect to SVE data confirm the qualitative comparisons illustrated in Fig. 12 (solvent A + CO_2 system), Fig. 13 (solvent B + CO_2 system), and Fig. 14 (solvent C + CO_2 system). As previously stated, this aspect can be related to the use of an unsuitable binary interaction parameter for the CH_4 + CO_2 system.

This conclusion can be supported by considering also the deviation between calculated and experimental compositions of the liquid and vapor phases at SLVE given in Table 15: deviations for the liquid phase are higher than those for the vapor phase. As illustrated by the reciprocal position of the experimental and calculated compositions of the liquid phase at SLE/SLVE shown in Figs. 17 – 19, it clearly appears that the position of the vertex of the SLVE triangle corresponding to the liquid phase is highly dependent on the position of the liquidus line originating at the solubility limit of carbon dioxide in liquid methane in the binary CH_4 + CO_2 system.

To the contrary, the binary interaction parameter tabulated in Aspen HYSYS® V10 for the N_2 + CH_4 system appears to be suitable in the temperature range of interest seeing that, as illustrated in Figs. 17 – 19, the VLE region develops starting from the horizontal edge of the ternary diagram that represents the equilibrium behavior of the N_2 + CH_4 mixture.

Finally, it seems that a suitable binary interaction parameter has been tabulated in Aspen HYSYS® V10 for the N_2 + CO_2 system, even if its effect cannot be sufficiently evaluated owing to the low content of nitrogen in the mixture (about 10% for all the points within Tables 7 – 12).

6. Conclusions and perspectives

With respect to the N_2 + CH_4 + CO_2 system, this work presents for the first time (i) VLE data at temperatures lower than the triple-point temperature of carbon dioxide, (ii) SVE data at temperatures lower than the saturation line of methane, and (iii) SLE data.

The experimental analysis of the thermodynamic behavior of three N_2 + CH_4 + CO_2 mixtures reveals that two are the main effects related to the presence of nitrogen in the mixture:

1) the solubility of solid carbon dioxide in both the vapor and liquid phases is reduced. First of all, this can be related to the fact that solid CO_2 is generally less soluble in nitrogen (approximately 1.4% at 180 K and 3.1% at 190 K at 4 MPa [49]) than in methane. Secondly, this decrease in the solubility of CO_2 in methane due to the addition of nitrogen is more evident in the liquid phase than in the vapor phase, and this can be related to the largest reduction of the density for the liquid phase with respect to the vapor phase;

2) the region of the temperature.vs.CO_2-composition diagram affected by the liquid phase is moved towards lower temperatures for increasing contents of nitrogen in the mixture. This is of course due to the fact that nitrogen is lighter than methane, which certainly implies higher costs for the liquefaction of natural or biogas rich in nitrogen. Furthermore, increasing amounts of nitrogen widen the temperature region of existence of the solid-vapor equilibrium and spread the temperature range of existence of the solid-liquid-vapor equilibrium.

As a result and considering values calculated with the model, for the solvent B studied in this work (5% N_2 + 95% CH_4), the temperature has to be decreased below about 187.3 K before the

vapor-liquid equilibrium takes place (about 190.3 K in case of pure methane). At this temperature, carbon dioxide can solidify if its global composition in the mixture is higher than 3.3% (4.1% in case of pure methane).

Similarly, for the solvent C studied in this work (10% N_2 + 90% CH_4), the temperature has to be decreased below about 184.5 K (6 degrees below the case of pure methane) before the vapor-liquid equilibrium takes place. At this temperature, carbon dioxide can solidify if its global composition in the mixture is higher than 2.6% (1.5% less than in the case of pure methane).

The phase equilibria measured in this work for the methane + carbon dioxide system are in qualitative and quantitative agreement with some of the literature data. In particular, the measured solubility limits of CO_2 at SLE agree with the majority of the literature SLE data in the whole investigated temperature range (175 K < T < 190 K).

At the same time and despite the quite good agreement between modeling results and VLE, SVE, and SLVE measurements, higher deviations have been encountered in the representation of measured SLE for the three systems by means of the thermodynamic package. Therefore, the regression of the binary interaction parameters (in particular for the CH_4 + CO_2 system), could lead to the improvement of the representation of SLE data (both from the literature and from this work) by keeping an appropriate representation of the other kinds of phase equilibrium.

In addition to the regression of new binary interaction parameters, in the next future authors will focus more deeply on the representation of solid-fluid equilibria by means of common process simulators. In particular, a further study will investigate Aspen HYSYS® and other commercial process simulators deviations against literature values and experimental values measured in the present work. In perspective, the final aim of the investigation will be the enhancement of the

process simulators capabilities through the development of reliable and ready for use tools enabling accurate prediction of solid phase formation.

Declaration of competing interests

The authors declare that they have no known competing financial interests or personal relationships that could have appeared to influence the work reported in this paper.

CRediT authorship contribution statement

Marco Campestrini: Conceptualization, Methodology, Experiments, Modeling, Writing. **Francesca Rabino**: Conceptualization, Methodology, Validation, Writing. **David Marques**: Experimental apparatus conception, realization, and testing. **Dyhia Atig**: Experiments, Modeling. **Paolo Stringari**: Conceptualization, Methodology, Validation, Supervision. **Guido Franzoni**: Conceptualization, Methodology, Validation, Supervision. **Barbara Picutti**: Conceptualization, Methodology, Validation, Supervision.

Acknowledgement

The Centre of Thermodynamics of Processes of MINES ParisTech, PSL University, is thankful to Maire Tecnimont for the financial contribution.

Nomenclature

VLE, Vapor-Liquid Equilibrium; SVE, Solid-Vapor Equilibrium; SLE, Solid-Liquid Equilibrium; SLVE, Solid-Liquid-Vapor Equilibrium; AAD, Absolute Average Deviation; MAD, Maximum Absolute Deviation

References

[1] British Petroleum Energy Outlook, **2020**, ww.bp.com

[2] Outlook for biogas and biomethane: Prospects for organic growth, **2020**, International Energy Agency, www.iea.org

[3] De Guido, G.; Messinetti, F.; Spatolisano, E. Cryogenic nitrogen rejection schemes: analysis of their tolerance to CO_2. *Ind. Eng. Chem. Res*. **2019**, *58(37)*, 17475–17488. doi.org/10.1021/acs.iecr.9b02544

[4] Rafiee, A; Khalipour, K. R.; Prest, J.; Skryabin, I. Biogas as an energy vector. *Biomass and Bioenergy*. **2021**, *144(105935)*, 1–20. doi.org/10.1016/j.biombioe.2020.105935

[5] Awe, O. W.; Zhao, Y.; Nzihou, A.; Minh, D. P.; Lyczko, N. A Review of biogas utilisation, purification and upgrading technologies. *Waste Biomass Valor*. **2017**, *8*, 267–283. doi.org/10.1007/s12649-016-9826-4

[6] Berstad, D.; Nekså, P.; Anantharaman, R. Low-temperature CO_2 removal from natural gas. *Energy Procedia*. **2012**, *26*, 41–48. https://doi.org/10.1016/j.egypro.2012.06.008

[7] Maqsood, K.; Mullick, A.; Ali, A.; Kargupta, K.; Ganguly, S. Cryogenic carbon dioxide separation from natural gas: a review based on conventional and novel emerging technologies. *Rev. Chem. Eng*. **2014**, *30(5)*, 453–477. doi.org/10.1515/revce-2014-0009

[8] Eggeman, T.; Chafin, S. Beware the pitfalls of CO_2 freezing prediction. *Chem Eng, Prog*. **2005**, *101(3)*, 39–44.

[9] Eggeman, T.; Chafin S. Pitfalls of CO_2 freezing prediction. *Proceedings of the 82nd Annual Convention of the Gas Processors Association*, San Antonio, Texas, **2003**.

[10] ZareNezhad, B. Prediction of CO_2 freezing points for the mixtures of CO_2-CH_4 at cryogenic conditions of NGL extraction plants. *Korean J. Chem. Eng.* **2006**, *23*, 827–31.

[11] Peng, D.-Y.; Robinson, D.B. A new two constant equation of state. *Ind. Eng. Chem. Fundament*. **1976**, *15*, 59–64. doi.org/10.1021/i160057a011

[12] Aspen Plus V10; Aspen Technology Inc.: Bedford, MA, **2017**.

[13] Prausnitz, P.; Lichtenthaler, R. N.; de Azevedo, E. G. Molecular thermodynamics of fluid-phase equilibria, second ed., Prentice-Hall, Englewood Cliffs, NJ, **1986**.

[14] Sarashina, E.; Yasuhiko, A.; Shozaburo, S. Vapor-liquid equilibria for nitrogen-methane-carbon dioxide system. *J. Chem. Eng. Japan*. **1971**, *4(4)*, 377–378. doi.org/10.1252/jcej.4.377

[15] Somait, F. A.; Kidnay, A. J. Liquid-vapor equilibriums at 270.00 K for systems containing nitrogen, methane, and carbon dioxide. *J. Chem. Eng. Data*. **1978**, *23(4)*, 301–305. doi.org/10.1021/je60079a019

[16] Al-Sahhaf, T. A.; Kidnay, A. J.; Sloan, E. D. Liquid + vapor equilibriums in the nitrogen + carbon dioxide + methane system. *Ind. Eng. Chem. Fundament.* **1983**, *22(4)*, 372–380. doi.org/10.1021/i100012a004

[17] Trappehl, G.; Knapp, H. Vapour-liquid equilibria in the ternary mixture N_2-CH_4-CO_2 and the quaternary mixture N_2-CH_4-C_2H_6-C_3H_8. *Cryogenics*. **1989**, *29(1)*, 42–50. doi.org/10.1016/0011-2275(89)90010-6

[18] Al-Sahhaf, T. A. Vapor-liquid equilibria for the ternary system N_2 + CO_2 + CH_4 at 230 and 250 K. *Fluid Phase Equilibria*. **1990**, *55(12)*, 159–172. doi.org/10.1016/0378-3812(90)85010-8

[19] Xu, N.; Dong, J.; Wang, Y.; Shi. J. High pressure vapor liquid equilibria at 293 K for systems containing nitrogen, methane and carbon dioxide. *Fluid Phase Equilibria*. **1992**, *81*, 175–186. doi.org/10.1016/0378-3812(92)85150-7

[20] Xu, N.; Dong, J.; Wang, Y.; Shi, J. Vapor Liquid Equilibria for N_2-CH_4-CO_2 system near critical region. *J. Chem. Ind. Eng. China*. **1992**, *43*, 640.

[21] Ottøy, S.; Neumann, T.; Stang, H. G. J.; Jakobsen, P. J.; Austegard, A.; Løvseth, S. W. Thermodynamics of the carbon dioxide plus nitrogen plus methane (CO_2 + N_2 +CH_4) system: measurements of vapor-liquid equilibrium data at temperatures from 223 to 298 K and verification of EOS-CG-2019 equation of state. *Fluid Phase Equilibria*. **2020**, *509*, 112444. doi.org/10.1016/j.fluid.2019.112444

[22] Haufe, S.; Mueller, H. D.; Tietze, G. Solubility of solid carbon dioxide in a methane-nitrogen mixture. *Chem. Thec. (Leipzig)*. **1972**, *24(10)*, 619–621.

[23] Agrawal, G. M.; Laverman, R. J. Phase behavior of the methane-carbon dioxide system in the solid-vapor region. *Adv. Cryo. Eng.* **1974**, *19*, 327–338. doi.org/10.1007/978-1-4613-9847-9_40

[24] Le, T. T.; Trebble, M. A. Measurement of carbon dioxide freezing in mixtures of methane, ethane, and nitrogen in the solid-vapor equilibrium region. *J. Chem. Eng. Data*. **2007**, *52(3)*, 683–686. doi.org/10.1021/je060194j

[25] Xiong, X.; Lin, W.; Jia, R.; Song, Y.; Gu, A. Measurement and calculation of CO_2 frost points in $CH_4 + CO_2/CH_4 + CO_2 + N_2/CH_4 + CO_2 + C_2H_6$ mixtures at low temperatures. *J. Chem. Eng. Data*. **2015**, *60(11)*, 3077–3086. doi.org/10.1021/acs.jced.5b00059

[26] Shen, T.; Gao, T.; Lin, W.; Gu, A. Determination of CO_2 solubility in saturated liquid $CH_4 + N_2$ and $CH_4 + C_2H_6$ mixtures above atmospheric pressure. *J. Chem. Eng. Data*. **2012**, *57(8)*, 2296–2303. doi.org/10.1021/je3002859

[27] Gao, T.; Shen, T.; Lin, W.; Gu, A.; Ju, Y. Experimental determination of CO_2 solubility in liquid CH_4/N_2 mixtures at cryogenic temperatures. *Ind. Eng. Chem. Res.* **2012**, *51(27)*, 9403–9408. doi.org/10.1021/ie3002815

[28] Riva, M.; Stringari, P. Experimental study of the influence of nitrogen and oxygen on the solubility of solid carbon dioxide in liquid and vapor methane at low temperature. *Ind. Eng. Chem. Res.* **2018**, *57(11)*, 4124−4131. doi.org/10.1021/acs.iecr.7b05224

[29] Lemmon, E.; Huber, M.; McLinden, M. NIST Standard Reference Database 23: Reference Fluid Thermodynamic and Transport Properties-REFPROP, Version 10.0, National Institute of Standards and Technology, Standard Reference Data Program, Gaithersburg, **2018**.

[30] Riva, M. Biomethane upgrading process: thermodynamic study of solid-liquid-vapor equilibrium for methane rich mixtures. PhD Thesis, PSL University, Paris, **2016**.

[31] Valtz, A. El Abbadi, J.; Coquelet, C.; Houriez, C. Experimental measurements and modelling of vapour-liquid equilibrium of 2,3,3,3-tetrafluoropropene (R-1234yf) + 1,1,1,2,2-pentafluoropropane (R-245cb) system, *Int. J. Refrig.* **2019**, *107*, 315–325. doi.org/10.1016/j.ijrefrig.2019.07.024

[32] Taylor, B. N.; Kuyatt, C. E. Guidelines for evaluating and expressing the uncertainty of NIST measurement results., Technical report, National Institute of Standards and Technology, Gaithersburg, MD, **1994**.

[33] Pikaar, M. J. A study of phase equilibria in hydrocarbon−CO_2 system. PhD Thesis, University of London, London, **1959**.

[34] Neumann, A.; Walch, W. Vapor-liquid equilibrium for CO_2/CH_4 in the low temperature region and low CO_2-content. *Chemie Ing. Techn*. **1968**, *40*, 241–244.

[35] Donnelly, H. G.; Katz, D. L. Phase equilibria in the carbon dioxide - methane system. *Ind. Eng. Chem.* **1954**, *46*, 511–517. doi.org/10.1021/ie50531a036

[36] Brewer, J.; Kurata, F. Freezing points of binary mixtures of methane. *AIChE J*. **1958**, *4*, 317–318. doi.org/10.1002/aic.690040316

[37] Cheung, H.; Zander, E. H. Solubility of carbon dioxide and hydrogen sulfide in liquid hydrocarbons at cryogenic temperatures. *Chem. Eng. Prog., Symp. Ser*. **1968**, *64*, 34–43.

[38] Brady, C. J.; Cunningham, J. R; Wilson G. M. *Gas Processors Association Research Report 62*, **1982**.

[39] Chang, H. L.; Kobayashi, R. *J. Chem. Eng. Data*. **1967**, *12(4),* 517. doi.org/10.1021/je60035a014

[40] Voss, G. PhD Thesis, Technical University of Berlin, Berlin, **1975**.

[41] Streich, M. N_2 Removal from natural gas. *Hydrocarbon Process*. **1970**, *49*, 86–88.

[42] Davis, J. A.; Rodewald, N.; Kurata, F. Solid-liquid-vapor phase behavior of the methane−carbon dioxide system. *AIChE J*. **1962**, *8*, 537–539. doi.org/10.1002/aic.690080423

[43] Im, U.K.; Kurata, F. Phase equilibrium of carbon dioxide and light paraffins in presence of solid carbon dioxide. *J. Chem. Eng. Data*. **1971**, *16*, 295–299. doi.org/10.1021/je60050a018

[44] Sterner, C. J. Phase equilibria in the CO_2-methane systems. *Adv. Cryog. Eng*. **1961**, 6, 467–474. doi.org/10.1007/978-1-4757-0534-8_49

[45] Langé S. Purification of natural gas by means of a new low temperature distillation process, PhD Thesis, Politecnico di Milano, Milano, **2015**.

[46] Sparks K. A.; Sloan E. D. *Gas Processors Association Research Report 71*. **1983**.

[47] Campestrini, M.; Stringari, P. Solubilities of solid n-alkanes in methane: data analysis and models assessment. *AIChE J.* **2018**, *64*, 2219–2239. doi.org/10.1002/aic.16071

[48] The DIPPR Information and Data Evaluation Manager for the Design Institute for Physical Properties, DIADEM Professional Version 8.0.2, **2016**.

[49] Sonntag, R. E.; Van Wylen, G. J. The solid-vapor equilibrium of carbon dioxide-nitrogen. *Adv. Cryog. Eng.* **1962**, *7*, 99–105. doi.org/10.1007/978-1-4757-0531-7_12

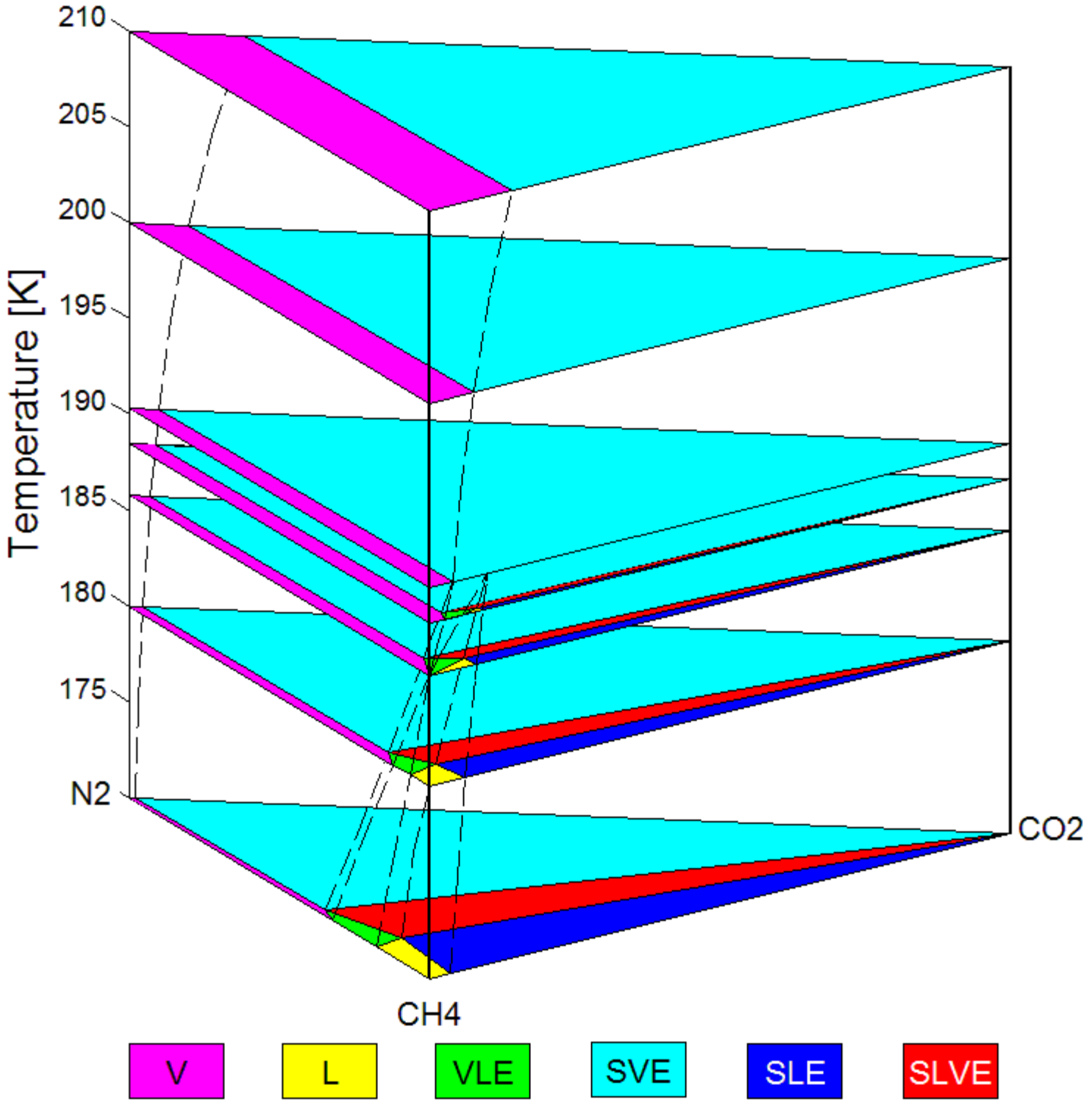
210
205
200
195
190
185
180
175
Temperature [K]
N2
CO2
CH4
V
L
VLE
SVE
SLE
SLVE